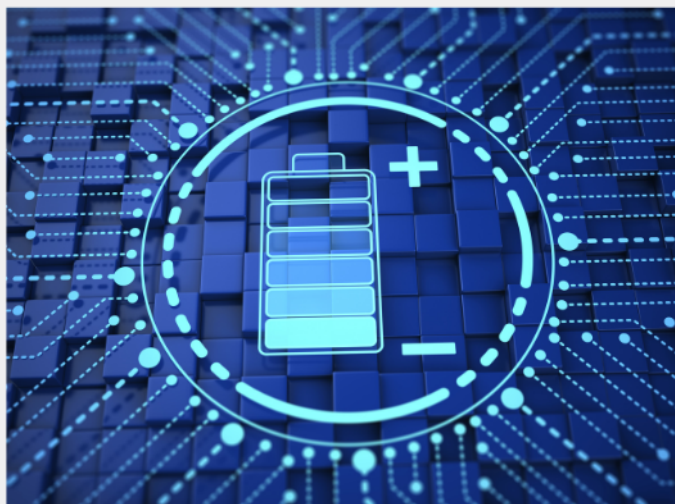




Exploring the possibilities of increasing energy density and efficiency in rechargeable batteries

Download this complimentary article collection



The exponential rise in the need for better, more efficient power sources has sparked an incredible amount of research into batteries. A primary focus of research has been increasing the energy density of batteries, as it allows for lighter, more portable storage of energy. Lithium-ion batteries, for example, have a much higher energy density than conventional lead-acid batteries and can be used for various purposes, such as in electric vehicles.

This article collection provides a comprehensive list of references for new methods and technologies for increasing the energy density of batteries.

2D Transition Metal Dichalcogenides-Based Electrocatalysts for Hydrogen Evolution Reaction

Aniruddha Mondal* and Alberto Vomiero*

Hydrogen is an efficient, clean, and economical energy source, owing to its huge energy density. Electrochemical water splitting is a potential candidate for inexpensive and eco-friendly hydrogen production. Recently, the development of 2D transition metal chalcogenides (TMDs) nanomaterials with a variety of physicochemical properties has shown their potential as eminent non-noble metal-based nanoscale electrocatalysts for hydrogen evolution. Nanostructuring such materials induces deep modification of their functionalities, compared to their bulk counterparts. High density of different types of exposed active sites is formed, and the small diffusion paths, which enhances the electron transfer in the 2D structures, can successfully aid the charge collection process in the electrocatalytic hydrogen evolution reactions. In this review, the key parameters to improve the catalyst performance of 2D TMDs in electrochemical hydrogen evolution reaction (HER) processes are discussed in detail and the most recent developments in the field are summarized, focusing on the improvement of the electrocatalytic activity of 2D TMDs. This review delivers deep insight for the clear understanding of the potential of 2D TMDs nanoscale materials as electrocatalysts for HER, suggesting the development of new type of catalyst with efficient activity in HER as well as other renewable energy fields.

hydrogen has the maximum gravimetric energy density with lower heating value 120 kJ g^{-2} .^[4–6] The H_2 gas can be used in various industrial fields, including petroleum, fuels in general, methanol production, catalytic hydrogenation, etc.^[7–9] Consequently, hydrogen (H_2) is a central materials among all energy resources, which can give a boost and enhance the economical and environment friendly prospect.^[10–13]

For the above-mentioned reasons, it is crucial to establish a method for producing hydrogen in a safe and large-scale plant. There are different ways for producing hydrogen.^[12] Three major technologies exist for H_2 production: 1) coal gasification,^[14] 2) water electrolysis,^[15] 3) methane reforming.^[16] The majority of hydrogen is generated by coal gasification and methane reforming, while only 4% is obtained through water electrolysis.^[17] Current hydrogen production still heavily relies on fossil fuels, resulting in global


1. Introduction

The use of fossil fuels is one of the most critical issues in our society: because of their limited amount, as well as the poisoning of living systems with hazardous compounds caused by their use.^[1] For this reason, it is very crucial to produce an emission free and sustainable substitute.^[2,3] In preceding years, because of its exceptionally high energy density, H_2 has emerged as a viable alternative energy resources.^[4] Notably,

warming and air pollution through exhaust gases. The use of an eco-friendly method to produce hydrogen is very important to reduce the environmental impact.^[18] Water electrolysis is the best option to minimize pollution. The most important processes in the production of hydrogen from water is known as the electrocatalytic hydrogen evolution reaction (HER). Water electrolysis kinetics are very slow to produce Hydrogen fuel. Efficient catalysts are needed to accelerate the catalytic activity or kinetics of water electrolysis.^[19] The most efficient metals are belonging to the precious metal platinum (Pt) group series and highly active catalyst toward the HER. However, the restricted abundance and unaffordable price of platinum (Pt) group metals have made them an expensive investment, less expensive and readily available catalysts would be preferred to catalyze HER. 2D TMDs may serve as an excellent material testbed for electrocatalytic, optoelectronic, energy storage and conversion, photocatalysis, magneto resistive, and thermoelectric device applications. In recent years, low cost transition metal-based nanostructures with different dimensions and shapes (e.g., 0D, 1D, 2D, and 3D) such as transition metal oxides (TMO),^[20–22] transition metal chalcogenides (TMD),^[23,24] transition metal carbides (TMC),^[25] transition metal nitrides (TMN),^[26] transition metal phosphides (TMP),^[27,28] and transition metal selenides (TMS)^[29] demonstrated their potential for catalytically active enhanced hydrogen production.

A. Mondal, A. Vomiero
Division of Materials Science
Department of Engineering Sciences and Mathematics
Luleå University of Technology
97187 Luleå, Sweden
E-mail: aniruddha.mondal@ltu.se; alberto.vomiero@ltu.se

A. Vomiero
Department of Molecular Sciences and Nanosystems
Ca' Foscari University of Venice
Via Torino 155, 30172 Venezia Mestre, Italy

 The ORCID identification number(s) for the author(s) of this article can be found under <https://doi.org/10.1002/adfm.202208994>.

© 2022 The Authors. Advanced Functional Materials published by Wiley-VCH GmbH. This is an open access article under the terms of the Creative Commons Attribution License, which permits use, distribution and reproduction in any medium, provided the original work is properly cited.

DOI: 10.1002/adfm.202208994

The catalytically efficient monolayers of TMDs are well performed nanostructured materials comprises potentials including metallic to insulating, which lead to the extensive applications, e.g., spintronics, optoelectronic, energy storage, electrocatalysis, heterogeneous catalysis, and photocatalysis etc.^[30–36] Specifically, these materials have well potential as substitute to the noble metal-based catalysts in electrocatalytic hydrogen evolution reactions.^[37] Among all the above-mentioned dimensional materials, 2D materials have a unique structure that makes them very appropriate for accomplishing the improved catalytic performance needed to tune the HER.^[38,39] In the widely open atomic surface of 2D nanostructured material, it is possible to optimize the quantity of active sites relative to the total number of atoms. In addition, surface modification of the 2D structure is an effective strategy to obtain high performance in HER, and 2D materials have maximized exposed surfaces in form of basal planes.^[28,40–46] Because of the distinctive properties of the 2D nanomaterials along with transition metal carbide and transition metal chalcogenides, numerous research efforts have been made to create effective 2D nanostructures toward electrocatalytic HER, mainly based on the fundamental mechanisms outlined in **Scheme 1**. Different approaches have been adopted including enhancement of electronic conductivity, increase of the density of active site of the catalyst and engineering of the catalyst at nanoscale level.^[47,48]

In short, in Scheme 1a,c,f, nonmetal doping, metal doping, and defect chemistry have led to better electrocatalytic performance than the undoped counterpart. In Scheme 1b, a large area 2D monolayer of metal chalcogenides with a large domain size, high thickness, uniformity, continuity, and good crystallinity was prepared using the CVD method; in **Figure 1d**, the interfacial engineering has shown a significant effect on the efficient electrocatalytic hydrogen evolution reactions.^[28,42,46,48–51] However, liquid exfoliation is a convenient, less expensive, and high yield strategy to get the single-layer 2D metal chalcogenide materials for accelerated electrocatalytic HER reactions. However, the generation of strain and edges has also helped to improve the efficiency of the 2D metal chalcogenide-based materials for the HER process (see Scheme 1g,h).

As an example, increased density of active sites can be obtained by applying plasma treatment, using Ar plasma, thin MoS₂ nanosheets layer by layer down to monolayer, increased density of exposed edges, and extensive defects.^[52–59] In another point, different paths have been investigated for enhancement/speed up the kinetics of the charge transfer processes owing to different architectural changes of the catalyst, including nanocomposites with highly conducting parts, doping of heteroatoms, strain in their basal plane, etc.^[52–59,45–51]

In this article, to review the electrocatalytic HER activity of 2D transition metal chalcogenide-based nanoscale materials, we extensively discussed their specific advantages and features. The critical points for further enhancement in electrocatalytic HER in this class of nanomaterials is discussed in detail. We also highlight the potential of Earth abundant and inexpensive 2D materials for efficient HER. The aim of this review paper is to give an insightful view into the 2D nanoscale catalysts based on transition metal dichalcogenides for electrochemical HER and pinpoint the most promising research directions in the field.

2. Basic Feature of HER

In electrocatalytic water splitting is nothing but a thermodynamically aided uphill strategy, whereas electricity is being used as a primary energy resource for water splitting. In **Figure 1a**, the two half reactions HER and OER occur at Cathode and Anode, respectively and requiring the overpotential with respect to their Thermodynamic values. The corresponding polarization curves and Tafel slopes for HER and OER process in the cathodic and anodic part. Several review papers summarize the basic features of HER in both acidic and alkaline mediums, Cathode and Anode part (in **Figure 1b**)^[78–82] For the synthesis of highly efficient HER electrocatalysts, several key characteristics are sought. The starting point is about the Gibbs free energy, which is tightly connected to the HER mechanism. Via electrocatalysis, H₂ can be produced via two methods in acidic medium,^[78,79,83–86]

The mechanism of electrocatalytic HER can be understood in terms of two main steps: i) the Volmer–Tafel step and ii) the Volmer–Heyrovsky step.

The first one is the Volmer Step, which includes the absorption of hydrogen on the catalyst surface by the simple blending of proton and electron:



Followed by a hydrogen evolution reaction:

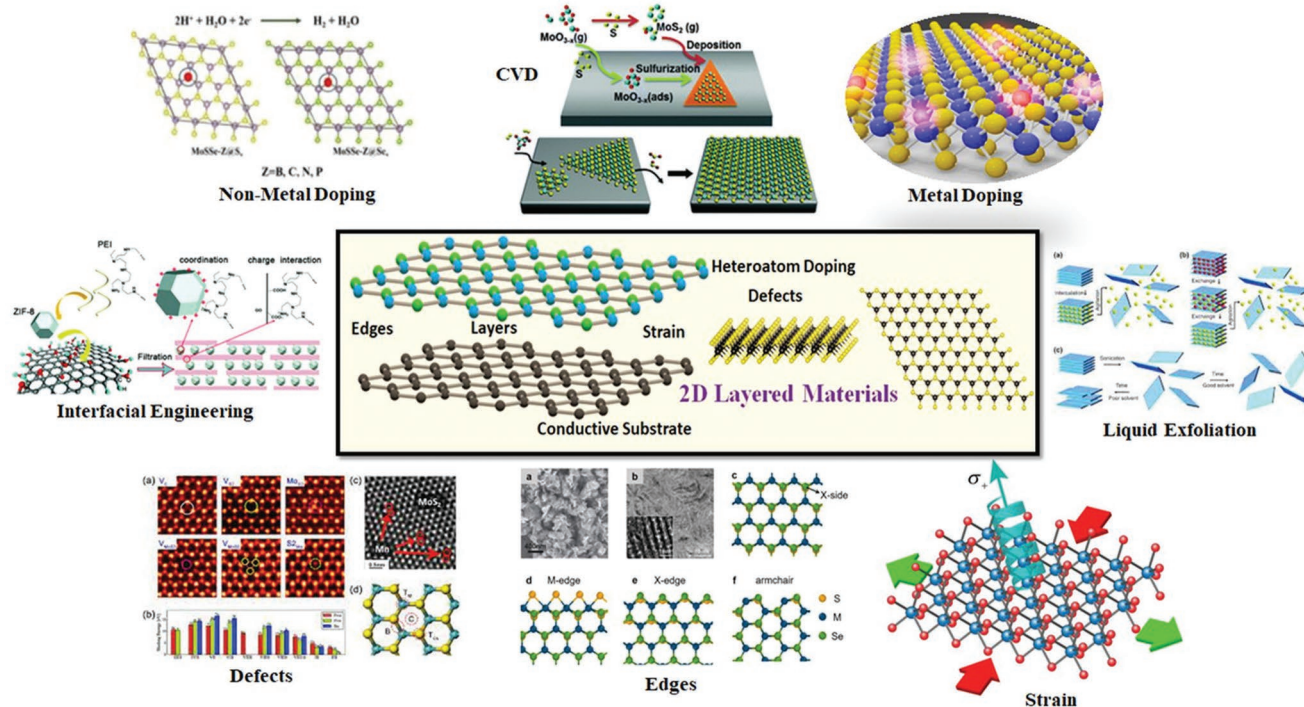


With the integration of two hydrogen atoms that have been adsorbed on the surface of a modified electrode, the H₂ gas evolves. The adsorption pattern of the hydrogen atoms follows the Volmer–Tafel mechanism (shown in **Figure 1c**).^[78,84,85,87,88] Additionally, the formation of hydrogen gas might be possible through the Volmer–Heyrovsky step:



The pre-adsorbed hydrogen atoms on the electrode surface associate with proton from the solution that formed H₂ gas as bubble: this process is well known as Volmer–Heyrovsky mechanism, which is shown in **Figure 1c**. In several electrocatalytic system, the Heyrovsky and Tafel slope may occur together.^[59,78] The “H” adsorbs in each and every step, so it is well acknowledged that Gibbs free energy for hydrogen adsorption (G_{EH}^{*}) is considered as a representative parameter for electrocatalytic hydrogen evolution catalyst.

In general, a number of variables, e.g., exchange current density (J₀), which is related to the Gibbs free energy of the individual catalytic system, are used to measure the electrocatalytic reaction activity for HER(**Figure 1c**).^[78,89] In volcano plot, the relationship between J₀ and G_{EH}^{*} is reported. The platinum series metals are at the peak of the volcano plot.^[90–92] Additionally, the adsorption energy for hydrogen is close to zero, which is indicative of their maximum catalytic performances. In volcano plot, elements on the right side of Pt series have lower G_{EH}^{*}, which indicates that it is very hard to stabilize the intermediate phase and as a result hydrogen



adsorption would be ineffective. This leads to the unproductive adsorption of hydrogen on the surface. In addition, for left side metal group of the Pt group, the G_{EH}^* is quite high, which lead to the poisoning of the corresponding catalyst surface, hence degrading the catalytic active surfaces. The G_{EH}^* can be used for the further evaluating non-metal catalytic systems. If we consider Molybdenum based materials, MoS_2 has shown the very low G_{EH}^* value compared to Pt, which resulted in highly efficient HER electrocatalysts. that G_{EH}^* evaluation is accepted as a reliable criterion for identifying materials that are excellent electrocatalysts in the hydrogen evolution reaction.^[78,93]

In a second point, highly efficient electrocatalysts are characterized by minimum overpotentials in electrochemical hydrogen evolution reaction, reduced Tafel slop, and enhanced exchange current density in electro-catalytical water splitting.^[94–97] Generally, four kinds of electrochemical reactions happen during water splitting reaction. The production of hydrogen gas during water splitting requires an overpotential greater than the potential value of 1.23 V (reversible electrolysis cell voltage), which is required in practice.^[17] In electrochemical water splitting reaction, the thermodynamic potential is 1.23 V at room temp. (25 °C). But because of their kinetic barrier for water splitting reaction, it requires more potential compared to the thermodynamically potentials, i.e., 1.23 V to cross the kinetic barrier. This additional potential is well known as the overpotentials (η), i.e., originated from their intrinsic activation barrier that existed on cathode and

anode. So, it is critical to have an extra overpotential to accelerate electron transport in attempt to improve the high activation energies resulting from the diverse chemical intermediates on the modified electrode surfaces. If the modified electrodes are subjected to a greater voltage, the water molecules that have attached themselves to the electrode surfaces break into hydrogen and oxygen at the cathode and anode, accordingly. The corresponding overpotential is calculated as well as Tafel slope.^[94] It is well recognized that the Tafel slope is a very significant critical point in determining the consistent current densities at a variety of overpotentials. In addition, it can be used extensively to assess the effectiveness of the electrocatalytic hydrogen production. Another vital parameter for kinetic studies, which is connected to the rate of electron transfer during hydrogen generation, is termed as exchange current density (j_0).^[96,97] In addition, in electrocatalytic hydrogen evolution reaction, other features and experimental techniques are important to be considered, including polarization curves, overpotentials, Tafel slopes, electrochemical impedance spectroscopy (EIS), exchange current density (j_0), chronoamperometry/chronopotentiometry, cyclic voltammetry curves, faradaic efficiency, and turnover frequency. Consequently, a summary of the most important parameters, which are typically considered in the evaluation of catalytic activity for water splitting, are reported in **Table 1**, including the overpotential, Tafel slopes, exchange current densities of 2D based materials that demonstrate their huge potential in electrocatalytic hydrogen evolution.

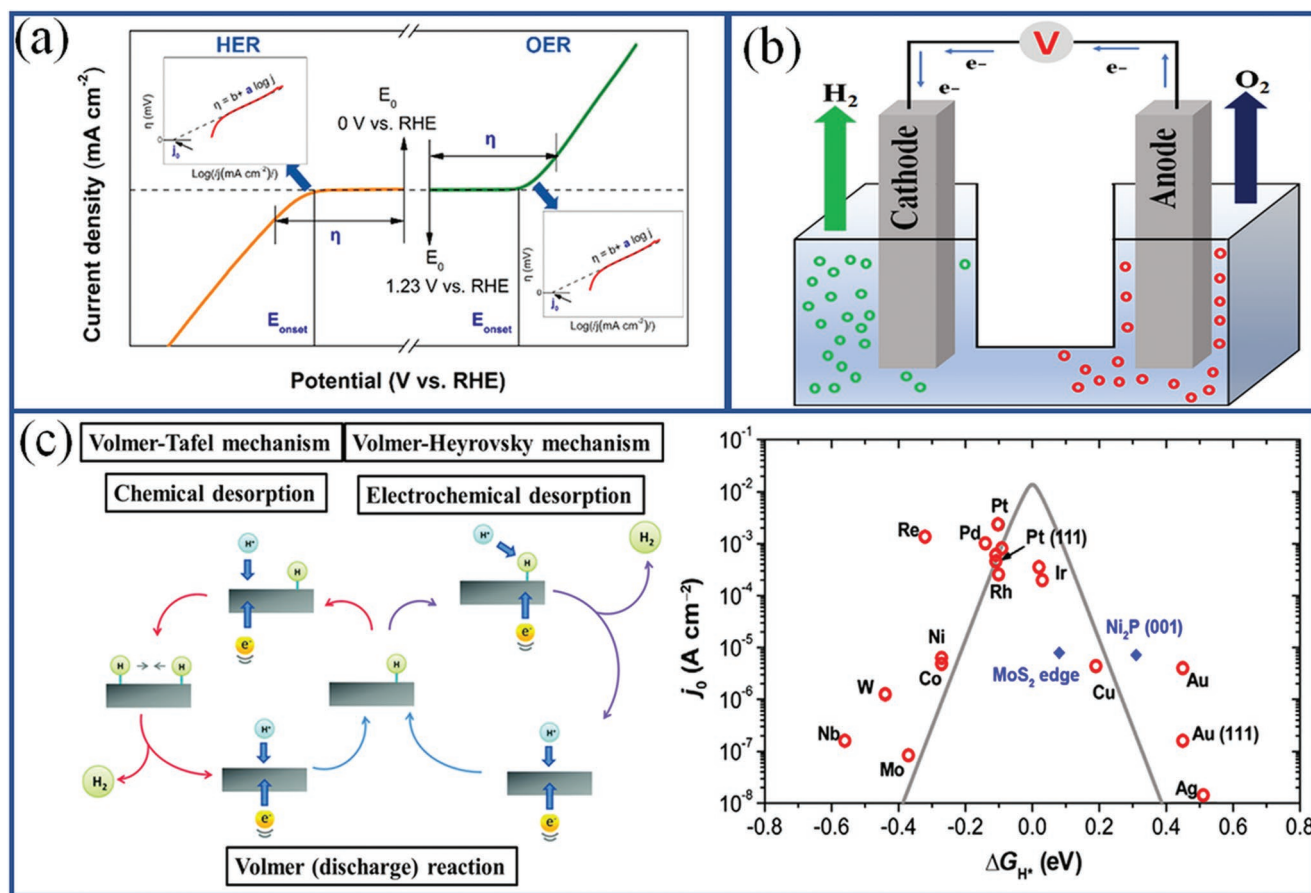


Figure 1. a) Polarization curves of two kinds of electrochemical reactions (Reproduced with permission.^[98] Copyright 2019, American Chemical Society). b) Diagrammatic view of the electrolyzer, c) Two types of mechanisms of hydrogen evolution in acidic media (Reproduced with permission.^[99] Copyright 2014, Royal Society of Chemistry). The volcano plot of exchange current densities against DGH (Reproduced with permission.^[91] Copyright 2017, Taylor & Francis).

3. Impact of 2D TMDs nanoscale materials in HER

For the assessment of the catalyst for hydrogen generation, 2D nanostructured materials have drawn a great attention as a well capable electrocatalyst in electrocatalytic HER than 1D and 3D category of electrocatalyst. Numerous parameters are important, such as atomic level thickness plane, high surface area, edge effects, topological effects, short ion diffusion distance, alleviated restacking, efficient charge transfer, and abundant active sites, which could be a diverse advantage in favor of HER.^[40,42,154–157,43,44,46,47,89,90,152,153] Bulk 2D based materials can be straightforwardly exfoliated into atomically thin layer sheet, including single and/or double layer, owing to the presence of weak van der Waals force between the layers, which can be easily separated with minimum efforts depending on their different physicochemical properties such as density, conductivity, corrosion resistance, melting point, and chemical stability.^[12,40,154,155,157,42–44,47,87,89,90,152] In case of transition metal based chalcogen materials, the transition metal atoms and chalcogen atoms would be exposed in their top position of the materials where electrolyte can access the active surface easily.

For this, Bonde et al. have effectively calculated the free energy on the edges of Molybdenum (Mo) and Sulphur (S) atoms in MoS_2 .^[158] Later, Nørskov et al. improved the corresponding values even more.^[159] The finding has demonstrated that the reactive part is found in Sulphur (S) and Molybdenum (Mo) edges, with Mo edges having a lower G_{EH}^* value. Therefore, several catalytic sites are possible in atomically thin facet. Furthermore, the large surface area of the 2D based nanomaterials can act as perfect platform to combine with other materials to form super active nanocomposites. Additionally, to generate surface defects,^[160] strain and different heteroatom, doping could be a unique way to activate and optimize the catalyst toward higher HER activities. Finally, such a perfect system with a small dimension is advantageous for researchers since it allows them to investigate and detect the best catalytic mechanism.

In the meantime, 2D materials could be a great model to show or set up a solid assembly with the open active sites along with the electrocatalytic activity of hydrogen evolution reaction. Even though, the 2D based electrocatalyst are considered as an excellent material for HER, However, their efficacy remains inferior to that of Pt-based materials in terms of effectiveness. The primary reason is due to the minimum access of different

Table 1. Comparison of the catalytic performances of different types of emerging 2D TMDs in HER.

Materials	Electrolyte	Current density [mA cm ⁻²]	Exchange current density [mA cm ⁻²]	Overpotential [mV]	Tafel slope [mV dec ⁻¹]	Reference
Co _{0.85} Se/graphene	0.5 M H ₂ SO ₄	10	–	250	41.8	[100]
MoS ₂	0.5 M H ₂ SO ₄	10	126.5	300	55	[101]
vanadium doped WS ₂	0.5 M H ₂ SO ₄	10	0.33	148	71	[102]
MoS ₂	0.5 M H ₂ SO ₄	10	–	170	60	[103]
Mo _{1-x} Nb _x Se ₂	0.5 M H ₂ SO ₄	10	–	140	46	[104]
MoS ₂	0.5 M H ₂ SO ₄	100	–	–	60	[105]
MoS ₂	0.5 M H ₂ SO ₄	10	0.6×10^{-4}	–	140	[58]
Ni _{0.85} Se/MoSe ₂	1 M KOH	10	–	108	77	[106]
MoS ₂	0.5 M H ₂ SO ₄	10	3.81×10^{-2}	300	61	[107]
MoS ₂	0.5 M H ₂ SO ₄	10	3.89×10^{-2}	–	68	[108]
ReSe ₂ @rGO	0.5 M H ₂ SO ₄	10	–	145	40.7	[109]
MoS ₂	0.5 M H ₂ SO ₄	10	–	118	46	[110]
Cu ₂ S	1.0 M KOH	10	–	125	44.8	[111]
MoS ₂	0.5 M H ₂ SO ₄	10	2.45×10^{-2}	100	73	[112]
MoS ₂	0.5 M H ₂ SO ₄	10	1.58×10^{-2}	153	43	[113]
Co ₉ S ₈	0.5 M H ₂ SO ₄	10	–	149	70	[114]
MoS ₂	0.5 M H ₂ SO ₄	3–44	–	–	100–150	[115]
MoS ₂	0.5 M H ₂ SO ₄	10	–	78	53	[116]
MoS ₂	0.5 M H ₂ SO ₄	10	–	200	40	[117]
Rh–Rh ₃ Se ₄ /C	0.5 M H ₂ SO ₄	10	–	32	50	[118]
V-doped MoS ₂	1 M H ₂ SO ₄	10	–	130	69	[119]
MoS ₂ @OMC	0.5 M H ₂ SO ₄	10	–	178	60	[120]
NiS@MoS ₂	1.0 M KOH	10	–	208	62.4	[121]
MoS ₂ /CA	0.5 M H ₂ SO ₄	10	1.72	150	59	[122]
ReS ₂	0.5 M H ₂ SO ₄	10	–	142	64	[123]
VS ₂	0.5 M H ₂ SO ₄	10	–	–	159	[124]
CoS ₂	0.5 M H ₂ SO ₄	10	–	197	29.9	[125]
TaS ₂	0.5 M H ₂ SO ₄	10	–	200	135	[52]
FeS ₂	0.5 M H ₂ SO ₄	10	1.44×10^{-4}	217	56.4	[126]
MoS ₂ /graphene	0.5 M H ₂ SO ₄	10	–	143	64	[127]
MoSe ₂	0.5 M H ₂ SO ₄	10	–	179	78	[128]
MoSe ₂	0.5 M H ₂ SO ₄	10	–	–	62	[129]
V-doped MoS ₂	1 M H ₂ SO ₄	10	–	130	69	[119]
MoS ₂ @OMC	0.5 M H ₂ SO ₄	10	–	178	60	[120]
Ni ₃ S ₂ -NiS	1.0 M KOH	10	–	141	75	[130]
VS ₂	0.5 M H ₂ SO ₄	10	–	–	159	[124]
WS ₂	0.5 M H ₂ SO ₄	10	–	130 mV	45	[131]
TaS ₂ , TaSe ₂	0.5 M H ₂ SO ₄	10	–	120	–	[132]
MoS ₂ @FePS ₃	0.5 M H ₂ SO ₄	10	0.43	168	127	[133]
MoSe ₂	0.5 M H ₂ SO ₄	10	0.36	102	53	[134]
MoSe ₂	0.5 M H ₂ SO ₄	10	–	–	101	[135]
MoSe ₂ -ts@MoS ₂ -ts	0.5 M H ₂ SO ₄	10	–	186	71	[136]
MoSe ₂	0.5 M H ₂ SO ₄	10	2.11×10^{-2}	182	69	[137]
MoSe ₂	0.5 M H ₂ SO ₄	10	–	150	80	[138]
CoS ₂ /CoSe@C	0.5 M H ₂ SO ₄	10	–	164	42	[139]
MoSe ₂	0.5 M H ₂ SO ₄	10	3.8×10^{-4}	250	59.8	[140]

Table 1. Continued.

Materials	Electrolyte	Current density [mA cm ⁻²]	Exchange current density [mA cm ⁻²]	Overpotential [mV]	Tafel slope [mV dec ⁻¹]	Reference
MoS ₂	0.5 M H ₂ SO ₄	10	2.63 × 10 ⁻³	151	39	[141]
MoS ₂	0.5 M H ₂ SO ₄	10	–	284	97	[142]
MoSe ₂ -NiSe@carbon	0.5 M H ₂ SO ₄	10	–	154	76.3	[143]
MoS ₂ /Ni ₃ S ₂	1 M KOH mV	10	–	–110	83.1	[144]
MoS ₂ -WS ₂	0.5 M H ₂ SO ₄	10	–	–129	72	[145]
Co ₃ S ₄ @MoS ₂	0.5 M H ₂ SO ₄	10	–	210 mV	88	[146]
MoS ₂	0.5 M H ₂ SO ₄	10	–	165	55	[147]
Fe _{1-x} Co _x Se ₂ /RGO	0.5 M H ₂ SO ₄	10	6 × 10 ⁻⁴	166	36	[148]
MoS ₂ /MoO ₂	0.5 M H ₂ SO ₄	10	–	300	35.6	[149]
Mn-doped CoSe ₂	0.5 M H ₂ SO ₄	10	6.83 × 10 ⁻²	174	36	[150]
CoSe ₂ /MoSe ₂	0.5 M H ₂ SO ₄	10	–	218	76	[151]
Fe _{1-x} Co _x Se ₂ /RGO	0.5 M H ₂ SO ₄	10	6 × 10 ⁻⁴	166	36	[148]

active sites, inert basal planes, and less conductivity which are mainly responsible for the less active electrocatalytic HER process.

Different approaches have been taken to get 2D based nanomaterials as catalyst with enhanced catalytic activity in electrocatalytic HER. In case of HER system, the two main parameters which favor hydrogen evolution are the enhanced charge transfer and the materials' inherent catalytic activity. Since the motivating and manipulating surface of 2D nanostructured materials, numerous approaches have been employed relating to two key core features, i.e., cumulative dynamic sites, enhanced electrical conductivity, and enhanced electrocatalytic results in HER, which is revealed in Scheme 1. Owing to that, we will discuss the different paths and strategies for improving the electrocatalytic HER activity with modified 2D nanostructured materials as efficient electrocatalyst [141, 142, 161, 162 (Figure 2).

4. Different Synthetic Strategy for Efficient HER

In general, inherent enhanced catalytic performances and the ample active sites are key important point for efficient catalysis in electrocatalytic hydrogen evolution reaction. Relative to the bulk part, a primary benefit of the 2D nanostructured materials are the catalytic active sites in the atomic level nanosheets, which is appropriately exposed, e.g., in ultrathin metal chalcogenide-based nanoscale materials, generally the most active sites are originated from their metal edges (Mo from MoS₂) or non-metal edges (S from MoS₂), so very thin layer could be a game changer for their opening of exposed active edges or sites, which was rooted in their bulk phases.^[163–166] Owing to their exposed edges as an active site in their inert basal plane, it is highly important to control the way the edge sites are exposed and to be able to selectively create exposed edges and defect engineering which have been involved to modify the HER activity.^[167–169]

The literature survey revealed that exposed edges and defect sites can be controllable experimentally even at atomic level of the 2D based TMDs. The synthesis and investigation of the

nanoscale materials and to creating the active basal plane of 2D TMDs are still challenging. The next section describes the different approaches to the synthesis of 2D TMDs, which can be carried out through both top-down and bottom-up techniques.

4.1. Bottom-Up

An alternative approach is the bottom-up method, which has the potential of creating less waste to be more economical. Bottom-up techniques are a potential alternative for the synthesis and fabrication of low dimensional materials (in Figure 3b).

In contrast to top-down processes, bottom-up approaches have many advantages such as ultra-fine nanoparticles, controlled size and shape including nano-shells, and nanotubes etc., different synthetic parameter which can be controlled and have controlled to narrow size distribution and less expensive.^[171–175] In order to further understand their exceptional physicochemical properties, it is well implemented in different novel areas including electrocatalysis, energy storage, and solar cells, it is necessary to develop novel growth models and characterization methodologies. Crucial approaches for creation of thin layers may be divided into several categories including exfoliation of the bulk materials. Due the less strong van der Waals force in between the layers in bulk 2D materials of transition metal chalcogenide, exfoliation processes may be applied to get ultrathin nanosheets. However, because of the complication of the electrocatalytic reaction in alkaline and acidic conditions, the mechanism of HER is sometimes unclear. Direct CVD growth may also be utilized to create TMDs with various layers, which aids in the investigation of layer-dependent mechanisms in electrocatalysis.

The appearance of exfoliated and CVD produced MoS₂ monolayers is vastly different. The CVD material has a substantially stronger PL than the exfoliated material, and the mode locations in its Raman spectra are notably different from those of the exfoliated material. As a result, the conventional approach for determining the number of layers, as published by Lee et al.^[176–179] and based on exfoliated samples, does not yield quantitatively accurate results for MoS₂ generated by CVD in this study. The

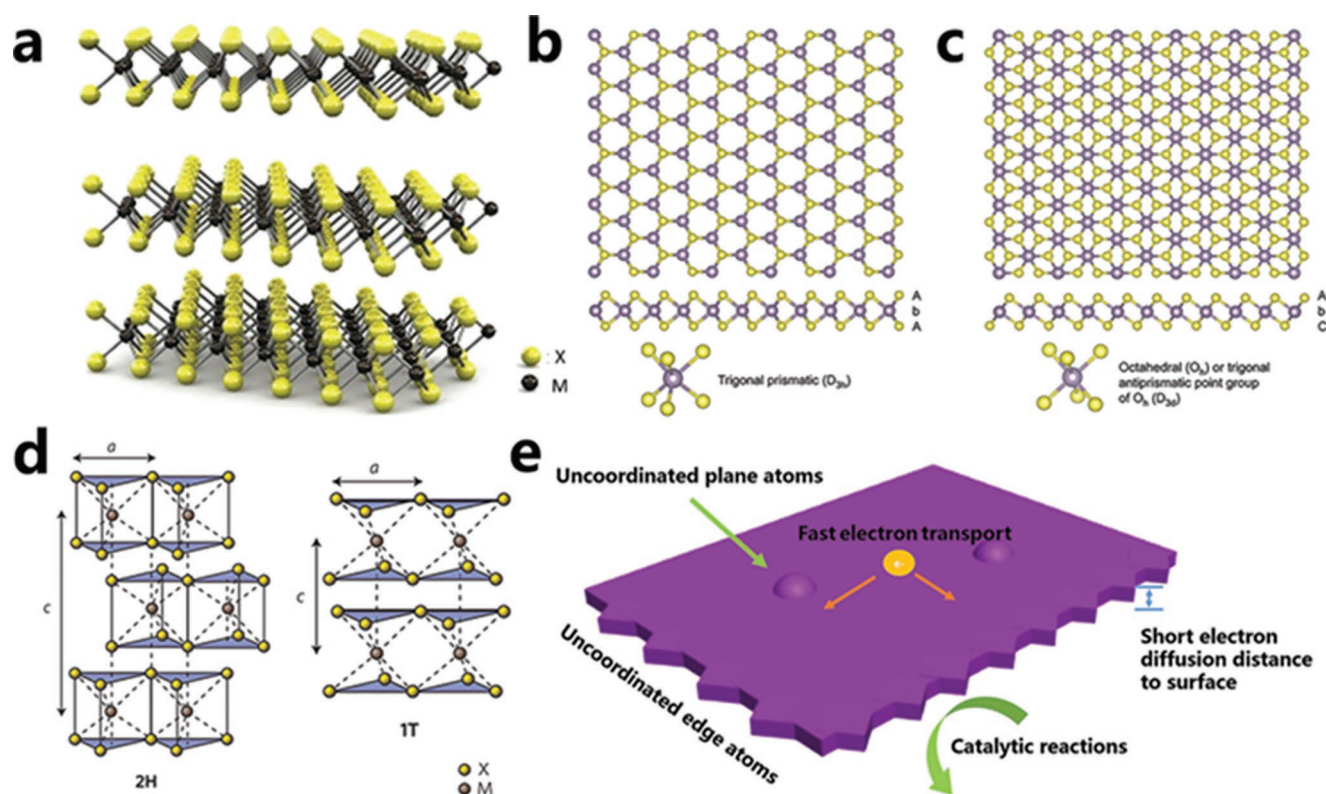


Figure 2. a, b) Structures of TMDs. (Reproduced with permission.^[161] Copyright 2019, Nature Publishing Group). Schematic representations of a typical TMD structure with trigonal prismatic c) Coordination from c- axis (upper) and section view (middle). (Reproduced with permission.^[141] Copyright 2013, Nature Publishing Group, d) (Reproduced with permission.^[142] Copyright 2012, Nature Publishing Group), and e) schematic illustration for the advantages of 2D TMDs as the electrocatalyst (Reproduced with permission.^[162] Copyright 2019, Nature Publishing Group).

following conclusions can be taken from our spectroscopic observations for different strain and doping values: When compared to exfoliated MoS₂, CVD produced MoS₂ looks to be more strained and less n-doped in comparison. According to the literature, the threshold voltage of CVD MoS₂ based field effect

transistors tends to be higher than that of transistors based on exfoliated MoS₂, which is consistent with these findings. Chemical vapor deposition is one of the most promising ways to meet these needs including defect and strain. Also discovered is that CVD operations using MoO₃ as a precursor often result in

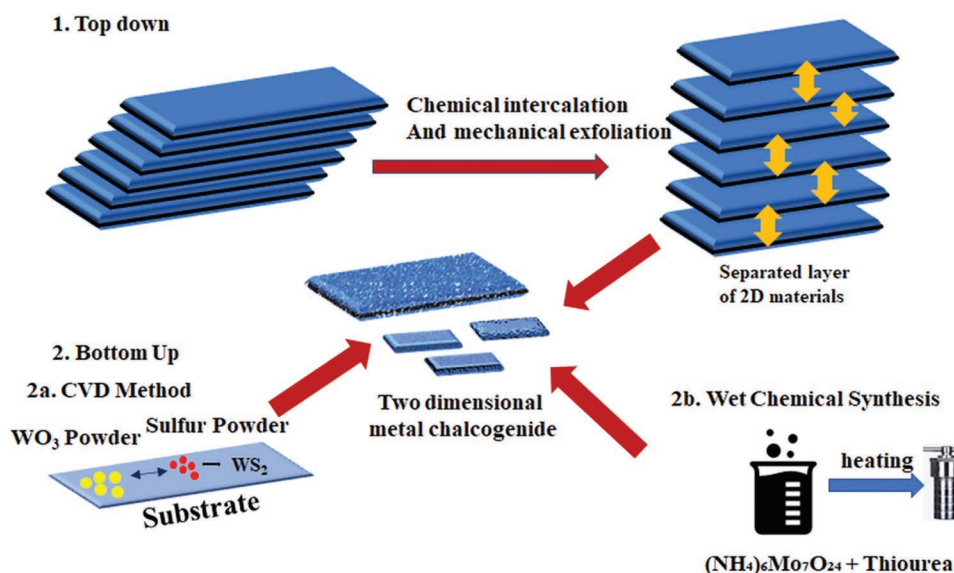


Figure 3. Schematic diagram of the a) Top down and b) Bottom-Up methods.

samples with a significantly greater range in terms of strain/defect density values than processes using other precursors. This demonstrates the superiority of the ammonium heptamolybdate precursor for the CVD development of MoS₂ and leads us to anticipate that, if the correct precursor can be found, a wide range of other 2D TMDCs may be produced with a similar level of quality.^[176] From the above points, a conclusion can be drawn that CVD grown TMD with multiple layers will help to find out the thin layer dependent in HER mechanism. In other hand, some other methods are employed to get few layers TMD, e.g., template assisted, ball milling strategy, and spray drying etc. In the next, we will debate on these processes to get more active sites for efficient electrocatalysis.

4.2. Top-Down

Top-down strategies initiate breakdown of the bulk materials into nanoscale size structures. For example, in top-down approaches different types of etching, intercalation, and direct patterning has been used to prepare 2D TMD nanoscale materials with different physicochemical properties. Details can be found in the exhaustive review by Stanford et al.^[170] As an example, using top-down approach 50 nm nanoribbon widths from its 2D TMDs, however it has significant challenges with this technique. At the time of Top-down processing, due to the etching processes at liquid and gas phase of the nanocrystals has been exaggerated towards the quality of crystal edges and basal planes.^[171–173]

Top-down approaches primarily consist of two methods: mechanical exfoliation and chemical exfoliation (in Figure 3a). In mechanical exfoliation, a monolayer or few layers can be exfoliated from the bulk 2D materials by using adhesive tape; generally, it is well known as the “Scotch tape” method. Using this strategy, many bulk 2D materials have been synthesized, such as boron nitride, graphene, metal chalcogenides, etc., as well as monolayers and few layers of 2D other materials, including metal chalcogenides. The synthesized 2D metal chalcogenides have shown excellent crystallinity and well-defined surfaces, which have prompted them for further fundamental research. The main drawback of this strategy is its low yield, which restricts large-scale production and further applications. The conventional method of mechanical exfoliation using Scotch tape consists of two steps.

The following two steps are

- 1) The primary action is to thin the bulky items, which were taped together using Scotch tape to reduce their size and continually removing them until the thick, bulky items are reduced in size to some degree.
- 2) The second step is to move the flaky exfoliant from the tape to the surface of a substrate by adhering tape to the substrate's surface.

Once the flakes are transferred, optical examination is utilized to determine their size and to select appropriate flakes for full characterization and device fabrication.

In chemical exfoliation, the main concept is to break the weak van der Waals force between the layers. Different

processes, like chemical-mechanical, chemical-thermal, and purely chemical, have been used to get single layers or few layers of 2D materials. In chemical exfoliation, most of the reactions take place in liquid. Chemical exfoliation has been used to produce a wide range of materials, including graphene, metal oxides, boron nitride, clays, metal hydroxides, and transition metal chalcogenides. There are two types of chemical exfoliation that have occurred during chemical exfoliation: ion intercalated and solvent aided. Colman et al. have proposed a unique way for solvent-assisted exfoliation processes to separate the MoS₂, MoTe₂, BN, Bi₂Te₃, etc.-based 2D materials from their bulk counterparts via the use of organic solvents (e.g., *N*-methyl pyrrolidone (NMP)). Another way is application of chemical and physical etching, whereas etching strategy is a very efficient top-down one to control the 2D materials (e.g., MoS₂) structure at their atomic level, along with the creation of fresh edges and pores. Many etching strategies have been used, including Ar⁺ plasma, AFM tip, laser methods are physical processes. In chemical methods, HNO₃, Cl[−], and O₂ have been used for reduced size and thin layer materials. Though, these strategies are mostly costly and hard to use. In addition, the chemicals involved in these processes may produce not uniform structures, other side products and contaminated materials, which will inhibit their further practical implementation. To minimize such issues, Zhang et al. have successfully exfoliated 2D MoS₂, a promising electrocatalyst for efficient electrocatalytic HER. In this approach, MoS₂ has been synthesized using sodium hypochlorite solution through anisotropic etching. Using this strategy, a defect free 2D MoS₂ with armchair architecture and uniform triangle pits are formed. The HER activity of the optimized MoS₂ catalyst has shown excellent HER performances, with an overpotential of 0.34 V and smaller Tafel slopes than other samples (such as O₂ plasma treated MoS₂) owing to their enhanced active sites.^[47]

4.3. CVD Methods

Exfoliation approaches are applied to obtain thin layer nanosheets from their bulk counterpart of TMD based materials. For instance, in MoS₂, more active sites have been revealed, which could be playing a key role to promote their electrocatalytic performances in HER. These methods have some drawbacks, including non-uniform number of layers, inhomogeneous size, and their complicated surface textures, which does not allow a full understanding of the basic mechanism for HER. The CVD method, which is best known for its controllable approach for fabrication of 2D materials, is broadly used to grow uniform ultrathin catalysts. CVD is able to deliver a very simple and well-controlled system for the systematic investigation of HER mechanism, including active sites and their catalytic action. Recently, Cao et al.^[58] established a path, i.e., dependence of HER on the number of nanosheet layers in MoS₂ grown via CVD on glassy carbon surface. The catalytic activity of the layered materials is related on their number of layers, as shown in Figure 4a, as a result of the layer dependence of the exchange current density (*j*₀). In fact, the catalytic performances of thin layer MoS₂ in HER increases by increasing their number of layers (Figure 4a). The charge transfer process was

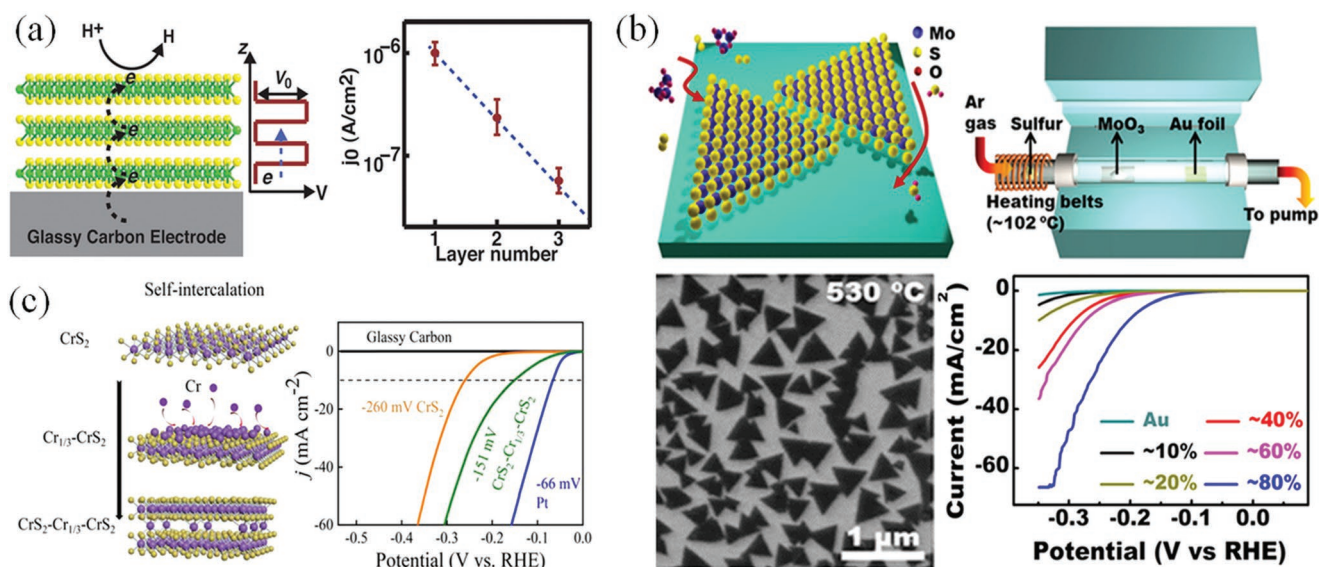


Figure 4. a) Schematic view of electrons hopping along the vertical direction in MoS₂ layers and polarization curves (Reproduced with permission.^[45] Copyright 2014, American Chemical Society). b) Schematic diagram describing the edges of single layer MoS₂ acting as the active sites for catalyzing HER, scanning electron microscope (SEM) of the as-grown monolayer MoS₂ on Au substrates polarization curves (Reproduced with permission.^[93] Copyright 2014, American Chemical Society). c) Schematic and self-intercalation diagram and polarization curves (Reproduced with permission.^[160] Copyright 2021, American Chemical Society).

simulated for gaining a clear concept of the electrocatalytic process occurring on the electrode surface. The quantum tunneling simulation for the electron transfer progress is reported in Figure 4a: when we observe on vertical direction of nanosheet layers, there is strong link between the exchange current density and the number of layers. The flowing electrons must pass through the working electrode to the external surface layer of the MoS₂ nanosheet to start the electrocatalytic HER. From this concept, it can be confirmed that the electrocatalytic HER happens only on the surface of the MoS₂. One good example, of the MoS₂ growth on Au surface over a low-pressure CVD was applied to obtain a single thin layer MoS₂ with homogeneous distribution (Figure 4b).^[107] The triangular shape of MoS₂ on Au surface has been compared in Figure 4b. The single layer MoS₂ nanosheet with maximum coverage has shown the minimum overpotentials and it presented a high current density at 300 mV overpotentials, i.e., 25 times higher catalytic activity than their bulk counterpart. Mainly, the edge length of the single layer MoS₂ materials can be altered from their bulk size (micrometer size to nanometer size) by changing their synthetic parameters including the temperature of the reaction conditions, and the minimum gap between the substrate and the electrode surface and the precursor source. Owing to that, a direct linear connection exists between the exchange current density and the edge length of MoS₂ crystals: this demonstrates that the electrocatalytic HER activity can be strongly endorsed with additional increase of the active sites. The growth of MoS₂ on gold surface is an effective strategy to obtain single layer electrocatalyst with rich active sites but it is not economical. Additionally, the strength of the MoS₂ grown on Au is restricted because of the weak interface cohesion between the grown catalyst and the conducting substrate. As we have mentioned earlier, to get highly rich active sites, ultrathin layer catalysts are needed, which can be grown through CVD. This strategy

represents a competent way for cultivating catalytic performances, which can be of help to probe the mechanism in electrocatalytic HER. Recently, Yuan et al. have fabricated CVD assisted of layered transition-metal dichalcogenides (TMDs) CrS₂-Cr_{1/3}-CrS₂ with excellent HER activity. With the CVD technique, to overcome the interlayer potential barrier of TMDs, CrS₂-Cr-CrS₂ is produced by simple self-intercalating Cr atomic plane in between the van der Waals layers of CrS₂, whereas the CrS₂-Cr-CrS₂ has shown strong chemical bonds along with improved conductivity, which is further accelerating the excellent electrocatalytic HER performances (in Figure 4c). The CrS₂-Cr-CrS₂ achieved a lower overpotentials value of 151 mV compared to the CrS₂ which is 260 mV at current density of 10 mA cm⁻².^[185]

4.4. Liquid Exfoliation

Liquid exfoliation of the bulk materials is a technique to obtain large scale production of atomic scale thin layer nanosheets. Due to that, multiple methods have been employed to get very thin layer nanosheet. Regarding this, the electrochemical lithium insertion processes to get 2D nano sheets from their bulk counterpart has been extensively implemented. Chhowalla et al.^[180] described the creation of monolayer of metal chalcogenide (WS₂) nanosheets for fastening the HER processes at minimum overpotentials through Li insertion into WS₂ materials. After intercalation with Li ion, the lateral dimension of these thin layer nanosheets decreased into the range 100–800 nm and their thickness were found to be around 1 nm only. These dimensions eased the creation of as much as active sites. Equally, such as very thin layer or monolayer of TiS₂ and TaS₂, using lithium intercalation, have shown more effective electrocatalytic activity compared to their bulk counterparts. Diverse

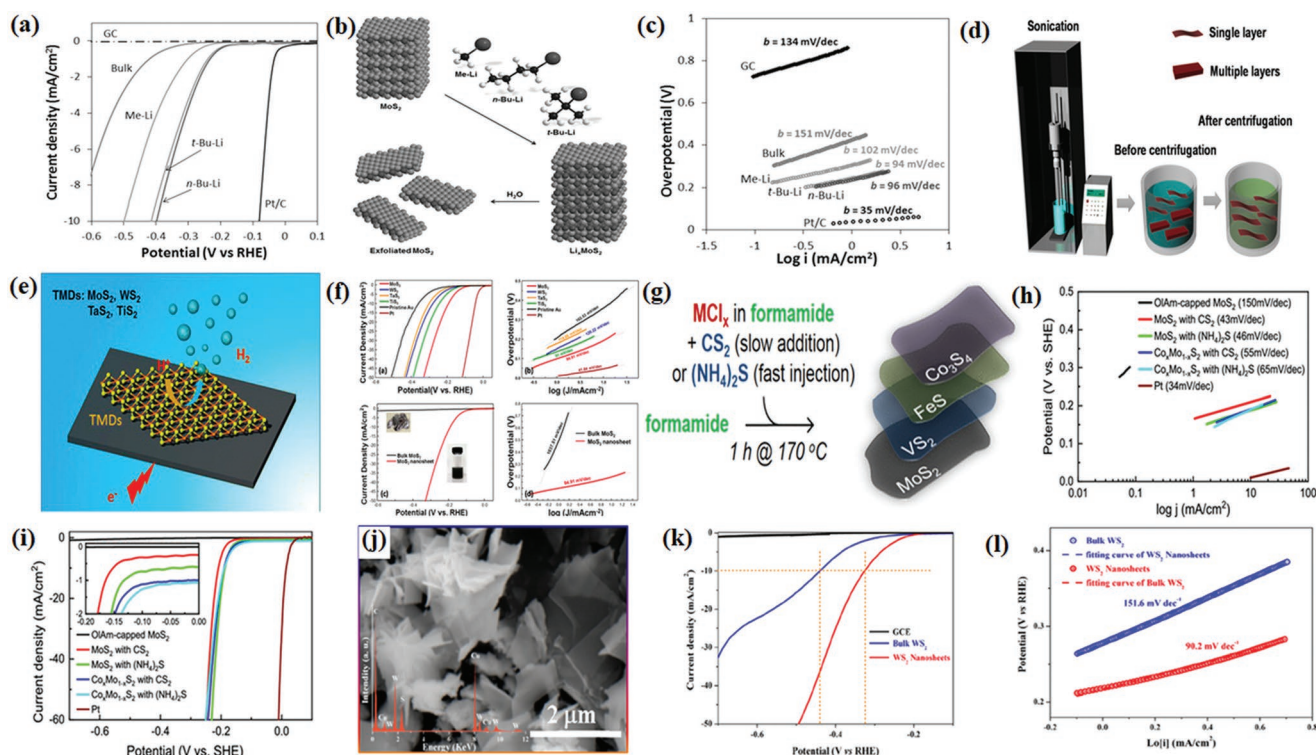


Figure 5. a) Polarization curves b) schematic diagram of the exfoliation of MoS₂ with three different organolithium compounds and c) Tafel plots of exfoliated MoS₂ nanosheets with three different organolithium compounds (Reproduced with permission.^[156] Copyright 2014, Wiley-VCH GmbH). d) Schematic view of the exfoliated MoS₂ via ultrasonication for catalyzing HER. e) Schematic diagram of TMDs and f) polarization curves and Tafel plots of TMDs, respectively (Reproduced with permission.^[157] Copyright 2016, American Chemical Society), g) scheme of the synthesis of TMDs, h) Tafel plots of TMDs i) polarization curves of TMDs (Reproduced with permission.^[158] Copyright 2020, American Chemical Society). j) SEM images of exfoliated WS₂ nanosheets k) polarization curves of WS₂ l) Tafel plots of WS₂ (Reproduced with permission.^[159] Copyright 2021, Wiley-VCH GmbH).

intercalation technique will give different density of active sites, which is instigated from the consequent various thin layers and sizes. Pumera et al.^[181] demonstrated that three alternative organolithium compounds, such as n-butyllithium (n-Bu-Li), tert-butyllithium (t-Bu-Li), and methylolithium (Me-Li) can be successfully applied for the split-up of bulk MoS₂ (Figure 5a–c). It is shown that, using n-Bu-Li and t-Bu-Li improved performances are obtained compared to the Me-Li. Specifically, when inserted with comparatively large size of organic molecules, the MoS₂ nanosheets has shown outstanding results toward HER. The key reason behind this excellent activity is the larger organic molecules, which are more stable and possibly will enable the intercalation of lithium ion. This has resulted in a reduction in the number of layers of the exfoliated MoS₂ nanosheet. Very recently, there have been reports of liquid exfoliation without the use of Li ions. Kim et al.^[182] has shown few layers of TiS₂, TaS₂, MoS₂, and WS₂ nanosheets (Figure 5d–e) using simple ultrasonication. From the polarization curves and Tafel slopes (Figure 5f), it is clearly indicated the changes of the HER performances between bulk MoS₂ and single layer MoS₂. In order to enhance the maximum exposed active sites, compact size of the single layer nanosheet of 2D materials could enhance the specific surface area, which lead to the enhanced HER performances. Very recently, Meerbach et al.^[183] has designed a general synthetic route to fabricate transition-metal disulphide nanomaterials as electrocatalysts for HER. Precisely,

the group has successfully synthesized different 2D materials without any organic ligand, e.g., VS₂, NiS, FeS, and MoS₂. Due to the number of innovative synthesis approach has possessed several advantages, like good reproducibility, yields, scalable processes, mild reaction conditions, and thermal treatment to increase the electrocatalytic efficiency of metal dichalcogenides. In case of Molybdenum disulfide nanosheets to increase the electrocatalytic activity of HER, the above points are helpful to get the efficient electrocatalyst. To establish the different synthetic approach, Co_xMo_{1-x}S₂ nanosheets in simple way to improve the electrocatalytic performances of MoS₂ based doped materials, these phenomena cause efficient HER activity with minimum onset potentials of 134 mV and small Tafel Slope of 55 mV dec⁻¹.

In Figure 5h,^[183] Tian et al. has fabricated the few layers of 2D WS₂ via simple lithium-ion intercalation exfoliation. With this technique, WS₂ nanosheets comprises enhanced lattice structure, no impurities, and increase lateral size. By this synthetic strategy, ultra-thin layer WS₂ nanosheet has added more active sites compared to their bulk counterpart, which lead to the more effective electrocatalytic activity. The exfoliated WS₂ nanosheets has shown improved overpotential value (320 mV at 10 mA cm⁻² (Figure 5k–l)) compared to their bulk counterpart. Thin layer WS₂ nanosheets has shown a low overpotential (320 mV at 10 mA cm⁻² (Figure 5k–l)) value compared to WS₂. However, to enhance the electrocatalytic performance

of the 2D nanosheets materials, Li intercalation exfoliation strategy is an excellent way to get few layers metal chalcogenides nanosheets.^[184]

4.5. Other Methods

Aside to the above-mentioned approaches, there are some few other efficient methods, which can be used to synthesized efficient catalyst for effective electrocatalytic hydrogen generation. Possible methods include ball milling,^[108] spray drying,^[59] template assisted synthesis,^[186] and can be implemented to get ultrathin nanosheets with different types of active sites. Ball milling will deliver a microdomain reaction: e.g., Wilkinson et al. have successfully synthesized 2D MoS₂ based nano catalyst with higher concentration of active sites (Figure 6a), than their bulk counterpart.^[108] The synthesized 2D MoS₂ via ball milling has its own ultrathin nanosheets: the extra small thickness of the MoS₂ basal plane leads to larger geometric surface areas. In Figure 4b, it is shown that all the synthesized MoS₂ nanosheet have better results, compared to bulk MoS₂. There have been many different templates used to create thin layer nanosheets with numerous active sites and increased electrical conductivity for electrocatalytic hydrogen evolution reaction (HER). These include mesoporous silica, 2D porous polymers, and 3D nanoporous gold.^[187,188] Implementing a template may assist in producing assemblies of few layer 2D materials with the highest density of exposed catalytically active sites and the

greatest possible increase in catalytic activity. In other points, different synthetic approaches offer us to explore the efficient HER, depends on the number of layers that can provide a scientific clue to design the advanced catalysts for enhanced HER. Joo et al. has created the MoS₂@ordered mesoporous carbon by utilizing mesoporous silica as an inorganic template and found out the HER performances are dependent on the number of layers.^[120] From theoretical point of view, with the help of density functional theory (DFT), ΔG_{H^*} was calculated for one, two, and three MoS₂ layers, which is playing a key role for the further evaluating the HER performances. As it is shown in Figure 6b, calculations were made to determine the number of Mo and S edges present in such layer catalyst. From the HER measurement and DFT calculations, the turnover number (TOF) of the MoS₂@OMC for the HER was derived. The TOF value is reduced quasi-linearly with the increase in layer numbers. The TOF value of the different layer of MoS₂@OMC including single- and double-layer catalysts was 2.32 S at 200 mV, which has shown the best performances. The decrease in the number of layers leads to the more sulfur sites in the exposed edges; as a result, an enhancement in HER activity was recorded^[120] (Figure 6b).

Nguyen et al. successfully synthesized the hollow spherical WS₂ and measured their hydrogen evolution reaction performance. In this synthetic method, when the temperature has been lowered down from 40 to 25 °C the thioacetamide crystallized from the saturated solution. the obtained nanostructures represented as first cores for inducing the WS₂ hollow

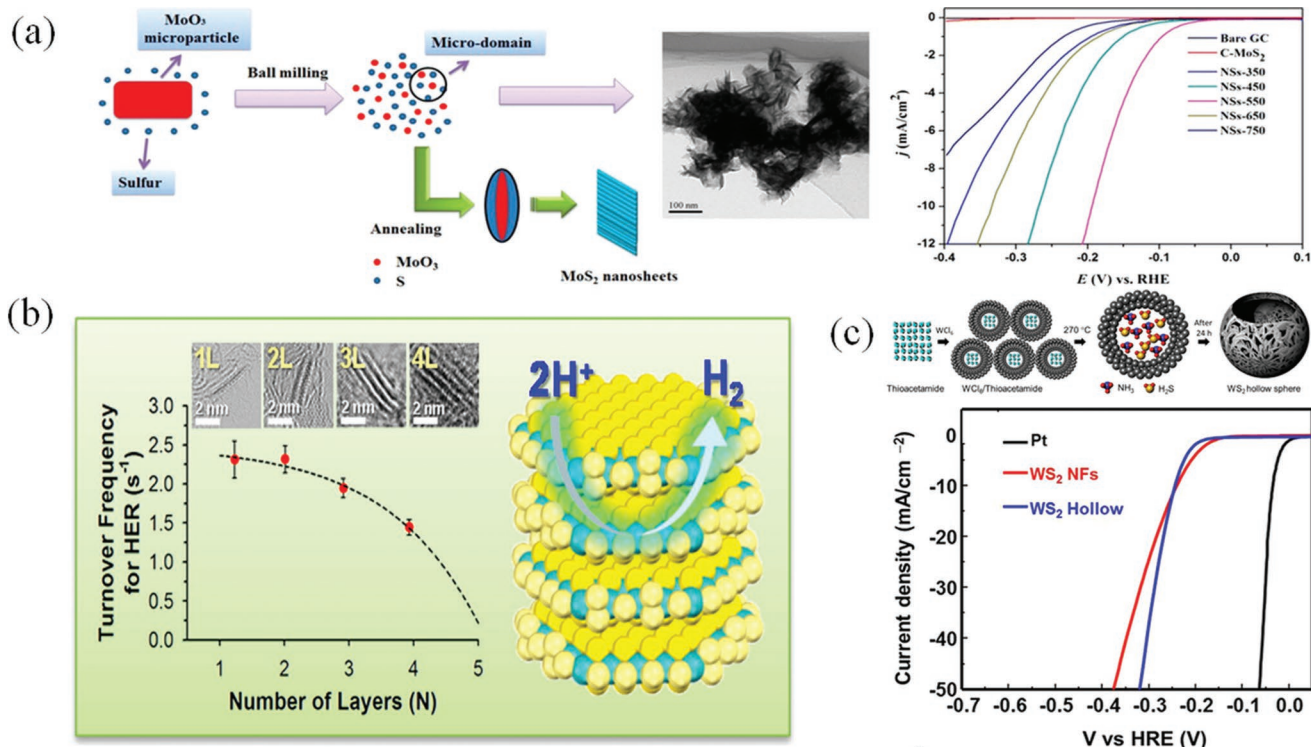


Figure 6. a) Schematic view of the ball milling process for synthesizing MoS₂ flakes and polarization curves (Reproduced with permission.^[94] Copyright 2013, American Chemical Society). b) MoS₂ structural model, favorable for HER on the basis of DFT calculations, the quasi-linear relationship between TOFs and the number of layers. (Reproduced with permission.^[106] Copyright 2015, American Chemical Society). c) Formation mechanism of WS₂ hollow spheres and polarization curves. (Reproduced with permission.^[164] Copyright 2020, Elsevier).

sphere. The diameter of the hollow sphere is around 300 nm to 2 μm . The performance of hollow spherical WS_2 as an efficient catalyst for electrocatalytic HER has been evaluated than WS_2 nanoflowers. Remarkably, WS_2 hollow structures (Figure 6c) showed higher onset potential and a Tafel slope of 125 mV and 60 mV dec^{-1} , compared to WS_2 nanoflowers (82.3 mV dec^{-1}).^[189] The approaches for the synthesis of thin layers, including CVD, exfoliation, sheet assemble hollow sphere, hydrothermal/solvothermal method, magnetron sputtering, spray pyrolysis, and ALD technique can successfully attain the synthesis of few layers and/or monolayers of TMDs. The overall active sites grew dramatically in correlation with the reduction in the number of layers, where more edges are easily available for high catalytic activities.

5. Role of Different Active Sites in HER

It is well known that maximum number of active sites of the 2D TMDs are situated at the edges of the materials, but in their basal plane does not have good catalytic activity. Efforts have been made to comprise different active sites such as defect and edge engineering of the basal surfaces of the thin layer materials in order to generate more effective electrocatalytic sites, like more corner atoms, kinks, terraces, and low coordination atoms, which are able to improve the HER activity.^[65,167–169,190]

5.1. Role of Edges

To regulate the surface construction at atomic level is the topmost criterion to develop emergent potential catalyst for hydrogen generation. Such as, the edges of sheet like MoS_2 have extremely catalytic active and as a result, MoS_2 basal

planes, which seem to be inactive, are preferred at their catalytic surface over surface active MoS_2 . Though, it is thermodynamically recommended the existence of basal planes as well as restricted effective sites for electrocatalysis on the surface. Superior catalytic efficiency for the HER is shown by the highly organized mesoporous morphology of MoS_2 with a controllable nanosheets layer. In fact, exceedingly well-organized double-gyroid MoS_2 bi-continuous matrix with different nanoscale holes were successfully synthesized by effectively tailoring the surface structure to selectively expose edge sites. Due to the fact that mesostructured-based materials have improved high surface curvature and surface area for electrocatalytic hydrogen evolution. Changing the MoS_2 morphology at nanoscale, by engineering the active edges of the MoS_2 surfaces, enabled the improved performances with very low overpotentials 150–200 mV.^[191] Additionally, making a vertically aligned nano scale architecture might also intensify the interaction with electrolyte in their exposed or opened edge sites. Metal chalcogenide-based materials including molybdenum chalcogenide (MoS_2 , MoSe_2) or tungsten chalcogenides (WS_2 or WSe_2) nanosheets can be assembled along the vertical alignment, it is possible to grow on the curved and abrasive surfaces of Si nanowires, carbon nanofibers, carbon fabric, and other materials (Figure 7a–c). The obtained overpotentials of the edge selective ultrathin film grown on such surfaces were much lower compared to common substrates such as glassy carbon electrodes (Figure 7c). It is very important to highlight that the effective edges of the nanosheets would be limited because of the unavoidable aggregation. Xu et al. has successfully fabricated the MoS_2 -C hybrid electrocatalyst for efficient HER with maximized S edges density, whereas the employment of the carbon-based aerogel materials with multiple irregular structures could stop further agglomeration through the synthesis of MoS_2 . Vertically oriented MoS_2 nanosheets can also be obtained, and

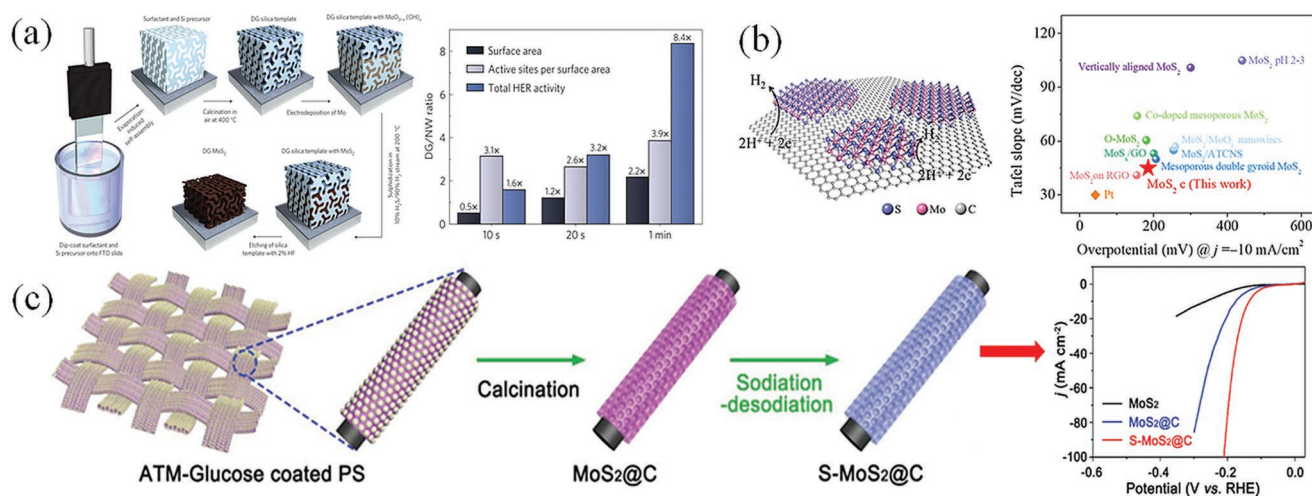


Figure 7. a) Synthesis procedure and structural model for mesoporous MoS_2 with a double-gyroid (DG) morphology and Ratios of surface area, density of active sites per surface area and total HER activity of the various double-gyroid MoS_2 films versus the nanowires (Reproduced with permission.^[166] Copyright 2012, Nature Publishing Group) b) schematic illustration of the heterostructure combining single-layer fractal-shaped MoS_2 and single-layer graphene and the HER performances of the fractal-shaped single-layer MoS_2 (sample c) and Pt foil measured in this work, including two important parameters, overpotential η (mV vs. RHE) when $j = -10 \text{ mA cm}^{-2}$ and Tafel slope (Reproduced with permission.^[167] Copyright 2018, Elsevier). c) Schematic illustration of the preparation process and microstructure and polarization curves Reproduced with permission.^[168] Copyright 2019, Wiley-VCH GmbH).

usually they have shown improved catalytic performances with the enhancement of effective active edges (Figure 7c).

5.2. Role of Defect

In general, the basal plane of the different type of TMDs are catalytically inactive for electrocatalytic HER. Multiple reactive sites can be generated on the plane by providing different degrees of defects, which can then be used to excite the electrocatalytic of the plane. Consequently, electronic, and physicochemical properties of the base of TMDs catalyst can be altered accordingly.^[49,192,193] Furthermore, defects are very effective approach to accelerate the electrocatalytic efficiency of the basal planes. The most important aspects that affect HER performance when it comes to defect engineering are the different phases of catalytic site and their intensities in the basal planes or surfaces, including terraces, low coordinated atoms, different size of pores, corner atoms, and kinks, these properties can make the basal plane with more catalytically active edges, the quantity of the defects in basal planes may also have an influence on the catalytic performances based TMDs nanoscale materials.^[37,167,168,190,194–196]

Currently, plasma-based approach has drawn a widespread attention to increase the catalytic activity of inactive basal plane of the different TMDs. For example, Chen et al fabricated a highly dense porous at atomic scale of “2D” TaS₂ materials to enhanced the electrocatalytic activity^[52] (Figure 8a). Plasma has been used to induce formation of defects by the evaporation

of Ta and S atoms from their nanosheet surfaces, as a result maximum distorted structure have been growing on the TaS₂ nanosheet (see in Figure 8a). A detailed quantitative examination of the Ta atoms at the edges was performed, and it was discovered that the varied levels of defect concentrations have grown in tandem with the different plasma treatment times, resulting in an increase in electrocatalytic activity. As it is shown in Figure 8a, in different exposure time changing at from 5, 10 to 15 min, the overpotentials in HER dropped from 302 mV to 200 mV and then increased to 225 mV, respectively. With the help of Ar or O₂ plasma, different physicochemical properties including defects can be created by changing the electronic properties as well as increase the electrocatalytic activity of the inert basal plane of TMDs.^[54,197–200] Different quantity of irregular shapes with triangular holes have been formed along with Mo and S ended active edges after H₂ and O₂ plasma annealing to the single layer MoS₂, grown on the SiO₂/Si substrate. Though, the loading of synthesized materials were very low to get the maximum catalytic performances and the stability was not sufficient owing to their less strong interface between the catalyst and the SiO₂/Si substrates. Xie et al. synthesized via hydrothermal routes in the liquid phase that also played a key role in creating more defect rich MoS₂ nanosheets with the addition of thiourea. To obtain more defect-rich MoS₂ nanosheets, an additional thiourea must be added to the hydrothermal system. To get the highly defect rich structure, excess thiourea has played an important role as a reductant to change Mo(VI) to Mo(IV). With this approach, the optimum density of active sites in defect rich MoS₂ nanosheets

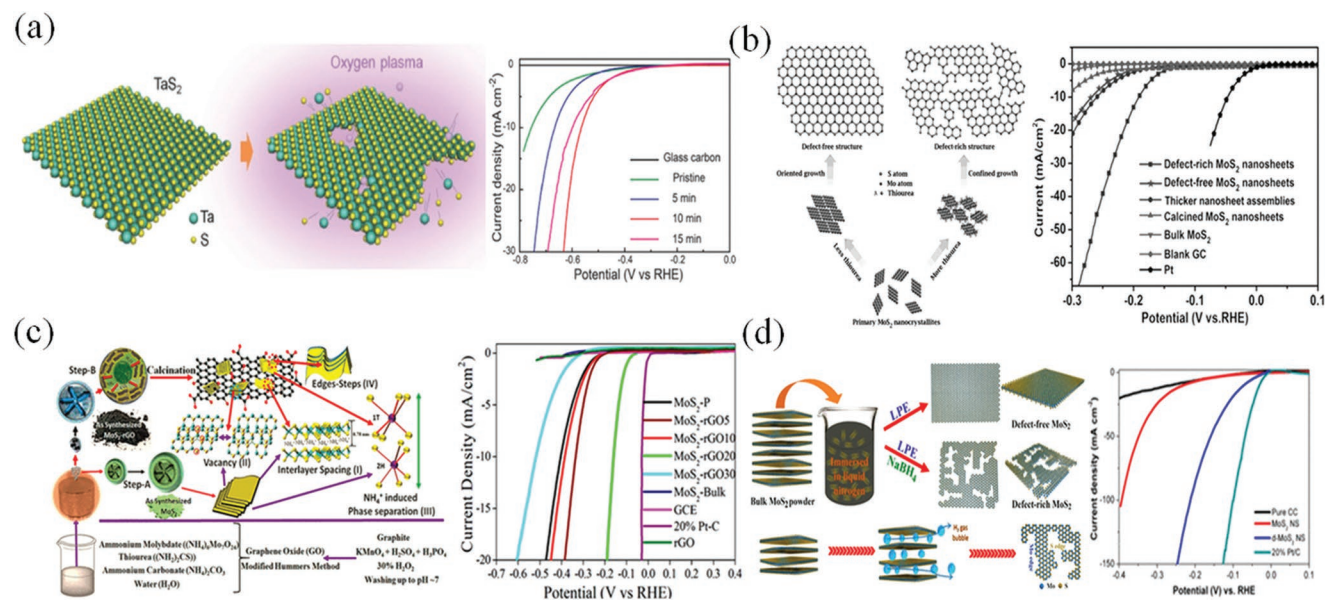


Figure 8. a) Schematic description of plasma treatment of ultrathin TaS₂ nanosheets and the formation of atomic-sized pores in the basal plane for enhanced catalysis toward hydrogen evolution and polarization curves (Reproduced with permission.^[39] Copyright 2016, Wiley-VCH GmbH) b) structural models of defect-free and defect-rich structures, as-designed synthetic pathways to obtain the above two structures and polarization curves (Reproduced with permission.^[176] Copyright 2013, Wiley-VCH GmbH) c) schematic representation of developed synthetic strategy for bare MoS₂ and MoS₂-rGO Nanocomposite Sheets and Corresponding Defects: I) enhancement of interlayer layer spacing for ammonium Ion Intercalation, II) generation of S vacancy, III) ammonium ion induced phase transformation from 2H to 1T, and IV) step edges and polarization curves (Reproduced with permission.^[46] Copyright 2018, American Chemical Society) d) schematic illustration of the synthesis process of cryo-mediated liquid phase exfoliation, the formation mechanism of the defect-rich MoS₂ NSs and polarization curves (Reproduced with permission.^[178] Copyright 2019, American Chemical Society).

was $1.785 \times 10^{-3} \text{ mol g}^{-1}$.^[201] Mondal et al. fabricated large-scale synthesis of MoS₂ based materials with graphene via spray dryer methods following calcination in inert environment. MoS₂ nanosheets with highly defect rich surfaces, the ammonium carbonate and thiourea has played a significant role.^[59] The spray dried assisted MoS₂ nanosheet has delivered overpotential of 168 mV and 62 mV dec⁻¹ (Figure 8c). Besides, Wu et al. developed a simple liquid exfoliation process for the production of ultra-thin and porous MoSe₂ based nanosheets, whereas H₂O₂ was utilized to exfoliate as an oxidant from their bulk counterpart to make single layer MoSe₂ ultra-thin highly porous structures. The obtained ultrathin, porous and highly defected MoSe₂ enhanced the maximum exposure of active sites and guaranteed a highly electrocatalytic performances toward HER (Figure 8d). The onset potential and Tafel slope for this system were calculated to be 75 mV and 80 mV dec⁻¹, respectively.^[138] Yang et al, reported the hierarchical spheres of defect rich MoS₂ through carbon via micro emulsion technique.^[202] CS₂ forms stable microemulsion along with PVP in aqueous system, which is served as Sulphur source as well as soft template. With the reversed molybdenum reaction mechanism, the S atoms are produced from the CS₂, S atom is diffused into the aquatic system, which further forms Mo-S-Mo interlink based compounds with additional S defects. In addition, in non-aqueous phase of CS₂, the ionic Mo (7+) does not able to insert easily, so, reversed molybdenum reaction produced maximum S defects in the corresponding compound, which further improve the electrocatalytic processes towards HER activity. The defect rich MoS₂/C hierarchical sphere has shown good electrocatalytic results with onset potential value -103 mV (vs RHE) with a Tafel slope of 56.1 mV dec⁻¹. The unique synthetic strategy helps to regulate the effective electrocatalytic sites of MoS₂. Zhang et al., describe a simple strategy for the synthesis of defect rich MoS₂ ultrathin nanosheet using NaBH₄ via cryo aided liquid phase exfoliation process (Figure 8d).^[203] As a result of the hydrophilicity of their surfaces and the availability of active edge sites, the electrocatalytic hydrogen evolution reaction (HER) performance of the d-MoS₂ NSs was significantly enhanced than MoS₂ NSs. Exploration of the impact of exfoliation time on the structural morphology of d-MoS₂ NSs with exposed edge sites provides an illustration of the synthesis process of these nanostructures. the best water-soluble molybdenum disulfide nanoparticles (d-MoS₂ NSs) had minimal overpotentials 71.5 mV at current density of 10 mA cm⁻², a low Tafel slope (58.3 mV dec⁻¹), and excellent cycle stability (>24 h).

6. Electron Transport Enhancement During HER

To enhance the electron transport for further improvement of the HER process, an ideal catalyst for electrocatalytic hydrogen evolution requires the presence of sufficient active sites as well as fasten charge transfer. Semiconducting 2D based TMDs nanomaterials demonstrate reduced conductivity, which restricts the HER kinetics. Consequently, new approaches for further increasing electron transportation for HER are highly interesting. Recently, different ways such as strain engineering, doping heteroatoms thermal treatment, and developing synergetic composites has gained a strong

interest since it has the potential to accelerate the overall catalytic kinetics of charge transfer. Moreover, few 2D based TMDs are inherently metallic, which is playing a key role to fasten the electron transport to accelerate the catalytic activity towards HER.^[50,59,204–207]

6.1. Strain Development

Owing to their atomic level thickness and enhanced elasticity, strain can be acquired in order to carry out lattice distortion of 2D materials.^[208–213] In order to increase the rate of electron transfer during hydrogen adsorption and desorption, it would be necessary to modify and enhance the d-band electronic structure in order to bring it near to the Fermi level. As a result, the distinction in gap states, which is generated by strain engineering, is one of the most important aspects of strain engineering during HER performances, e.g., the single layer of MoS₂ thin film has been grown on the surface of nanoporous gold which has strong external strain. The possible bending of the crystal lattices leads to the constant changes in the S-Mo-S bonding angles in MoS₂ layers, which produced a local semiconductor-to-metal transition in the MoS₂ monolayer^[110] (Figure 9a). Through S vacancies, Zheng et al. produced strain into 2H-MoS₂ (Figure 9b).^[103] The created S vacancies in 2H-MoS₂ directed to the construction of new valence bands, which are close to the Fermi level, permitting the hydrogen atoms to bind the exposed Mo atoms. Besides, when the tensile strain was implemented to create the S-vacancies, the position of these newly generated bands further shifted towards the Fermi level, which has given the smaller and as well as higher bandgap close to the Fermi level. The obtained Tafel slopes of the different category of MoS₂, MoS₂ with S vacancies and stretched MoS₂ with S-vacancies are calculated, i.e., 90, 82, and 60 mV dec⁻¹, respectively. These phenomena showed that the large strain is needed to get an effective catalytic activity. Zheng et al. has examined the kinetic mechanism of strained S vacancies of the surfaces of single layer MoS₂ via scanning electron microscopy (SECM). The electron transfer rate has been enhanced four times at 2% uniaxial tensile strain, which directly confirms that the tensile elastic strain can enhance the electrocatalytic kinetics of MoS₂ with S vacancies in HER (Figure 8b). Between uniaxial and biaxial tensile strain, biaxial tensile strain can help to improve the HER activity in more effective way. As per the first principles calculations, it has been guessed that the tensile strain would bring about the lowering the adiabatic proton affinity, as well as the enhancement in the adiabatic electron affinity, therefore resulting in an enhanced catalytic activity of HER. It was also possible to compute the total electronic structure of m-MoS₂ while it was in the 1H and 1T phases. It has been discussed that the tensile strain might be a highly effective way to trigger the inactive inner valence electrons and to enlarge the d-band exchange splitting, that plays a key role for the catalytic enhancement in HER. Furthermore, Kuo et al. examined the different 2D TMDs (1T-MX₂, M: Mo, W, etc. and X: S, Se, etc.) and strain engineering has shown very well performances in HER. Beside the tensile strain, an appropriate compressive strain possibly will enhance the electrocatalytic efficiency of 2D TMDs materials.

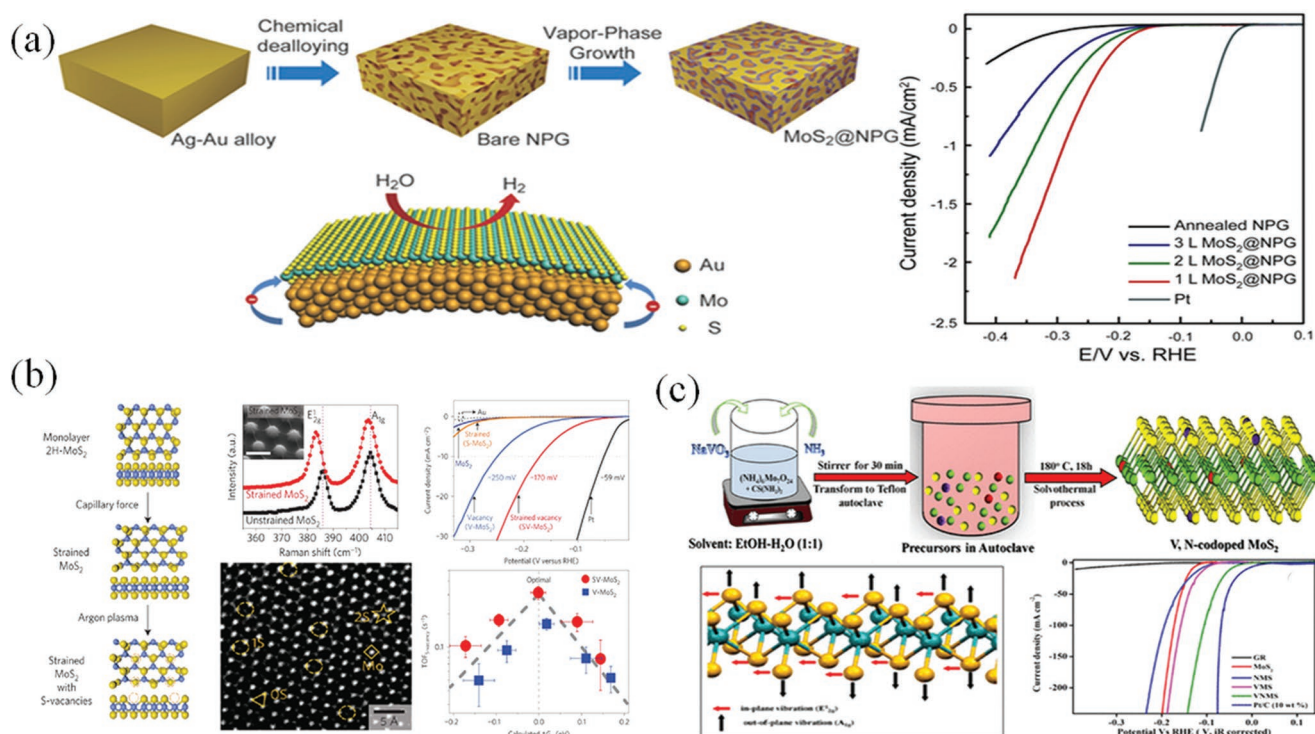


Figure 9. a) Schematic HER catalyzed by the monolayer MoS₂@NPG hybrid material and polarization curves (Reproduced with permission.^[96] Copyright 2014, Wiley-VCH GmbH) b) schematic of the top (top panel) and side (lower panel) views of pristine monolayer 2H-MoS₂, polarization curves and experimental TOF_{S-vacancy} versus their corresponding calculated ΔG_H for V-MoS₂ and SV-MoS₂ (Reproduced with permission.^[89] Copyright 2016, Nature Publishing Group) c) preparation of vanadium- and nitrogen-doped MoS₂ (VNMS) in the solvothermal method, represents the (001) HER active crystal plane and polarization curves (Reproduced with permission.^[191] Copyright 2021, American Chemical Society).

The density of states may decrease due to the internal compressive strain until it reaches the Fermi level and reduce the strength of hydrogen bonds to promote functional charge transfer and the electrocatalytic hydrogen evolution process (HER).^[214] Bolar et al. successfully synthesized strain MoS₂ thorough doping of V and N by simple solvothermal method.

By introducing crystal strain, altering charge transfer, and including a newly created (001) plane with improved H-adsorption capacity, V and N doped MoS₂ nanosheets has improved the overall catalytic performances. The Mo and S atoms in MoS₂ has been replaced by V and non-metal N atoms from their lattice points, which produce crystal strain.^[215] V and N doped strained MoS₂ has shown excellent results in HER with very low Tafel slope of 57 mV dec⁻¹ and with overpotential value of 122 mV at 10 mA cm⁻² (Figure 9c).

6.2. Doping Heteroatoms (Nonmetal-Doped Catalysts and Metal-Doped Catalysts)

Transition metal dichalcogenides (TMDs) are materials that have long been under attention; with the development of modern synthetic methods, it has become thinkable to study and use the monolayers of these compounds. The doping of various heteroatoms may cause the basal plane of TMD-based nanostructured materials to be distorted or enlarged the interlayer distance, therefore altering their d-band electronic properties

and diminish their hydrogen adsorption free energy changes (ΔG), which is solely responsible for the enhanced electrocatalytic HER processes. Here, doped TMDs based catalysts are separated into two section including metal doped and non-metal doped TMDs. It is possible that both of these types of heteroatoms doped nanoscale materials will increase the rate of charge transfer.^[58,190–195] Different metal atoms may be inserted into the architecture of the TMDs materials as co-catalysts to maximize WS efficiency. Xie et al. introduced manganese into Cobalt selenide (CoSe) nanosheet for enhanced HER^[150] in Figure 10a. the integration of the Mn with CoSe might accelerate the hydrogen atoms on their catalytic surfaces and then reduce their kinetic energy; as a result, might be more active sites developed, as seen by images from high resolution transmission electron microscopy (HRTEM). The doped CoSe have lower overpotential compared to the bulk CoSe. This technique has opened a workable way to obtain composite materials for the efficient electrocatalytic HER.^[150] It is also projected that the semiconductor MoS₂ will be possibly transformed to semimetal MoS₂ by V doping. Additionally, different defect sites can be formed by V doping, favored to meaningfully accelerate the carrier concentration, which has also been established by theoretical (DFT) calculations. The V doped MoS₂ is more effective for electrocatalytic HER catalyst compared to their bulk counterpart.^[119] Introduction of the different transition metals to alter the materials structural disorder, such as Co element, might enhance the density of overall active sites for HER catalysis. Jin

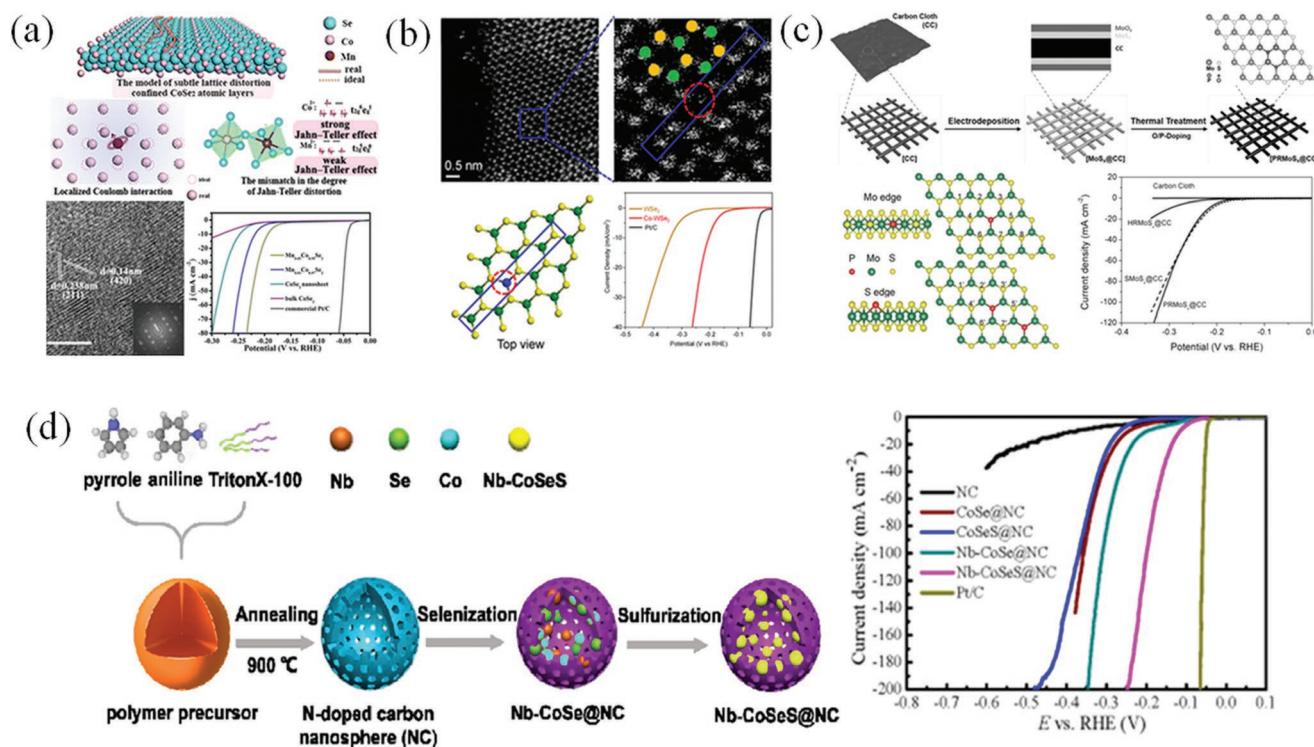


Figure 10. a) Schematic representations of the formation mechanism for the subtle distortion of atomic arrangement through the incorporated heterogeneous spin states, HRTEM images, FFT and polarization curves (Reproduced with permission.^[136] Copyright 2016, American Chemical Society). b) HAADF-STEM image of Co-WSe₂ nanosheets, the detailed images of the selected area, top view structure model of the Co-WSe₂ nanosheets and polarization curves (Reproduced with permission.^[198] Copyright 2021, American Chemical Society) c) schematic representation of the fabrication process of the P-doped 2H MoS₂ phase of PRMo_x@CC electrode, atomic structures of P-doped Mo-edge and S-edge of 2H phase of MoS₂, supercells of Mo₁₆S₃₁P and Mo₁₆S₃₀P₂. The numbers denote reaction sites and polarization curves (Reproduced with permission.^[47] Copyright 2017, Wiley-VCH GmbH). d) Synthetic process for Nb-CoSe@NC and polarization curves (Reproduced with permission.^[205] Copyright 2021, Elsevier).

et al. found that the Co element in different TMDs, including NiS, CoS₂, FeS₂, and their alloys is useful for enhanced electrocatalytic activity. The electrocatalytic enhancement will be modified as a result of the increase in Cobalt content, might act as a significant role in the enhancement of HER. In the meantime, Zhang et al. revealed a dynamic structural revolution in tungsten selenide after cobalt doping, which lead to the direct optimized electronic state of Se active sites, accelerating the H₂ production under HER. From the theoretical point of view, the rationality of the structural growth and the effect of doping on the Se active sites enhance the overall electrocatalytic water splitting, resulting in 140 mV at 10 mA cm⁻². With the Co doping effect, this work provided a clear understanding of the doping effect on accelerating the electrochemical performances^[220] (Figure 10b). Wang et al. have optimized the Molybdenum (Mo) doped into the rhenium sulfide nanosheet on carbon cloth. After Mo doping in ReS₂, the electronic structure of the materials has been improved along with their electrochemical performances. From the theoretical point, the Mo-ReS₂ and the bare ReS₂ materials density of states (DOS) is calculated, which shows that this material has behave as semiconductor with bandgap value of 0.47 eV. After Mo doped into ReS₂, the semiconductor materials turned into a metallic whereas metallic electronic structure is a p-type doping due to the redistribution of Molybdenum (Mo) 4d electron and the

charge transfer. From the above points, it can be explained that after doping of Mo atoms could be helpful to enhance the charge transport. This phenomenon has enhanced the overall performances of HER. The hydrogen evolution reaction electrocatalyst made of Mo-doped ReS_2 has been employed in acidic conditions with low overpotential values of 101 mV at 10 mA cm^{-2} , a Tafel slope of 40 mV dec^{-1} with outstanding stability.^[221] In order to achieve an enhanced electrocatalytic water splitting performances, nonmetal doped TMDs with a diverse variety of innovative characteristics have been implemented in conjunction with a nonmetal doped TMDs catalyst. Xiang et al. fabricated Se doped MoS_2 alloys (Se = 0.39, 0.51, and 0.61) through regulating the quantity of Se concentration in the MoS_2 semiconductor. As a result, optimizing the bandgap of MoS_2 nanosheets allows for the tuning of HER catalysts, that lead to a vital role in fine-tuning the conductivity of the newly synthesized catalyst.^[222] Mostly, the introduction of the Se atoms into thin layer MoS_2 nanosheets induces the formation of $\text{MoS}_{2(1-x)}\text{Se}_{2x}$, which exhibits larger ΔG than the pure MoS_2 or MoSe_2 , which can trigger the effective hydrogen separation from the monolayer surface of MoS_2 . The LSV pattern reveals that the onset potential of $\text{MoS}_{2(1-x)}\text{Se}_{2x}$ that is weaker than the onset potential of pure MoSe_2 or pure MoS_2 . From this investigation, it is also confirmed the positive doping effect in TMDs for enhance the HER.^[223] Mainly, because of the larger size of

Se than the S atoms, the insertion of Se atom into the WS₂ nanocrystals induces crystal distortion in the original structure, which creates a polarized electric field. Therefore, the polarized adsorbed reactants tend to be focused on owing to their induced electric field, which can play a key role in accelerating the bond breaking processes on the adsorbed water molecules. So, the monolayer of the Se-doped WS₂ has shown enhanced catalytic activity with minimum onset overpotentials of 80 mV, which is lower than that of undoped WS₂ and WSe₂. Additionally other types of TMDs nanosheets doped with Sulfur (S), Oxygen (O), and Hydrogen (H) atoms also showed improved performances.^[51,101] The conductivity of the materials would be enhanced owing to their declined bandgap energy, due to the presence of defects and strain originated from the S doping, which lead to the modified band gap energy of MoSe₂. The conductivity of MoSe₂ can be enhanced directly through decreased bandgap energy, which further improves the electrocatalytic performances of S doped MoSe₂, compared to the pristine MoSe₂.^[51] Additionally, O incorporation also represents an important strategy to control the electronic structure of the MoS₂ nanosheets, the obtained disorder in TMDs instantaneously gives additional unsaturated S atoms as an effective catalytic site,^[101] as shown in Figure 10b. The O incorporated MoS₂ have shown the excellent electrocatalytic activities. (Figure 10b) it can be deduced from their polarization curves and equivalent Tafel plots. To maximize the efficiency of metal elements as electrocatalysts, P doping was also used to change their electronic states.^[60,224] The electrocatalytic performances of HER of P doped MoS₂ has shown excellent activity, because of their noteworthy decrease in the valency of Mo after P doping, which leads to the lesser free energy changes, than the pristine MoS₂ basal planes (Figure 10c). In the past few years, MoS₂ has drawn a great potential as an effective electrocatalyst to drive HER, but in doped MoS₂ has hardly been described due to their hard-synthetic path. Yang et al. has successfully designed atomic scale substitution of Pd/O Co-doped into MoS₂, which exhibits very small onset potential of 23 mV at a current density of 10 mA cm⁻² with reduced Tafel slope of 18 mV dec⁻¹. From the theoretical study it is also confirmed that Pd/O doping in MoS₂ forms defect pairs in MoS₂ which are created due to added unsaturated S atoms around the defect sites, promoting the excellent HER activity.^[225] Chai et al.^[226] has shown that metal doping for active sites exhibits excellent HER activity. Nb doped CoSeS materials well doped in N-doped carbon nanosphere (Nb-CoSeS@NC) were synthesized to serve as a conductive substrate and enhanced their activity for HER. Nb doping can alter the electronic structure of the CoSe that fastens the HER processes. The synthesized Nb-CoSeS@NC, with unique core shell structure, shown a low overpotentials of 115 mV at 10 mA cm⁻² which is smaller than the other doped electrocatalyst in Figure 10d.^[226]

7. Fabrication of Synergetic Nanocomposites

To get intrinsic high catalytic activity of the poorly conducting 2D nanoscale materials, in order to speed up electrocatalytic hydrogen evolution processes, a few synergetic composite materials have been identified that boost or speed up the electron transport process.

7.1. Synergy with Conductive C-Based Materials

Carbon-based materials including carbon nanotube, graphene, carbon dots, and different carbon materials with outstanding electron transport ability along with high chemical stability have been assembled with 2D TMDs based nanoscale catalyst. The carbon-based materials can prevent further agglomeration and endorse the charge transfer processes.^[227–229] In addition, they increase the overall conductivity of the composite TMD-based materials, further improving the electrocatalytic kinetics for HER. The carbon-based materials have been coupled with 2D TMDs as cooperative catalyst to gain the overall kinetics of the HER processes. Dai et al. synthesized MoS₂ nanoparticles on reduced graphene oxides sheet via solvothermal technique. The obtained MoS₂/rGO hybrid materials possess the nanoscopic few layers MoS₂ structure, with a maximum exposed edge, which is stacked on the graphene sheets, compared to the aggregated MoS₂ particles, which are synthesized without reduced graphene oxide sheets. The synthesized MoS₂/rGO nanosheet has shown excellent electrocatalytic activity towards HER, compared to bare MoS₂ catalyst. The obtained MoS₂/rGO catalyst has shown Tafel slope 41 mV dec⁻¹, deriving from the excellent electrical coupling to the underlying graphene network. For better HER performances, when using a hybrid catalyst, such as MoS₂/rGO, the chemical and electrical interaction between the GO sheets and MoS₂ is enhanced. Due to the vastly well dispersed MoS₂ nanoparticles on the surface of GO is lead to the well-defined physicochemical coupling between MoS₂ and GO and the characterization of these phenomena are all being investigated. Since MoS₂ on GO is a small size and dispersed widely, it provides a large number of readily edges that are readily available to initiate the HER might function as active catalysts. Due to the strong coupling effect between MoS₂ and highly conducting graphene sheets lead to the fasten electrocatalytic processes during HER.

The MoS₂/RGO hybrid has a much lower impedance when measured at an overpotential of = 0.12 V than the pristine MoS₂ (Figure 11a). With the MoS₂/RGO hybrid catalyst, the drastically lower Z_f resulted in much accelerated HER kinetics than before.^[227] Coleman et al. assembled the MoS₂ nanosheet with single wall carbon nanotubes; as a result, the current density of the composites was increased after adding the carbon nanotubes. The main reason is that the active sites, originally inaccessible, can now be reached more easily through the highly conductive channels, thus improving the charge transfer.^[115] In general, the performance of the thicker MoS₂ electrode with more active sites is driven by electron transport rather than mass transfer, resulting in weak electrocatalytic activity. The insertion of SWCNTs, on the other hand, modified the transfer in the thick MoS₂ electrode more active in the direction of electrocatalysis than before. It is shown that (Figure 11b) at the same potentials, the thicker MoS₂ films had lower onset overpotentials and greater current density. Ramakrishna et al. constructed a flexible electrode made of CoS₂/rGO/Carbon nanotube nanocomposites.^[230] Carbon nanotube (CNT) and graphene both are conductive substrate, CNT network enhances the efficient charge transfer process. The CoS₂ nanosheet grown on the surface of rGO substrate led to the excellent interface as well as avoid aggregation and/or phase transformation,

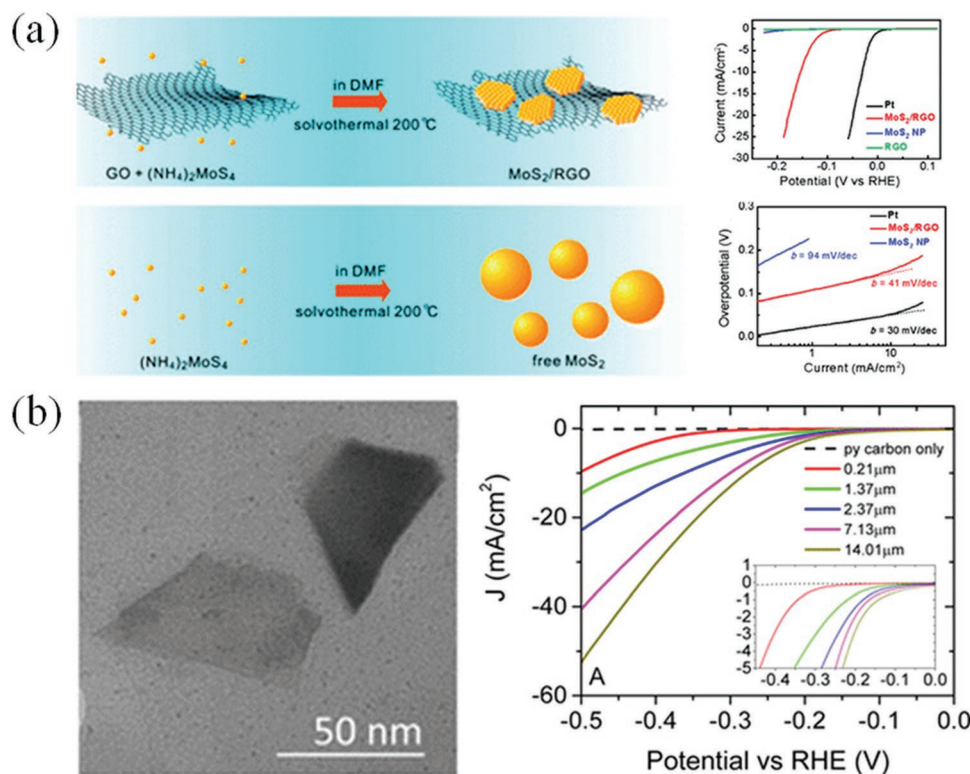


Figure 11. a) Synthesis of MoS₂ in solution with and without graphene sheets, polarization curves and Tafel plots (Reproduced with permission.^[206] Copyright 2011, American Chemical Society). b) TEM images of exfoliated MoS₂ nanoflakes and polarization curves (Reproduced with permission.^[101] Copyright 2016, American Chemical Society).

which lead to the excellent electrocatalytic performances of the CoS₂/rGO-CNT nanocomposites. Additionally, tin based TMDs have also attracted much attention, including SnS₂, SnS, SnSe, Sn₃S₄, etc. because of the excellent physicochemical properties enhances the catalytic activities.^[231–233] Lee et al. has shown the large-scale synthesis of SnS on N doped reduced graphene sheets. The presence of various functional groups in graphene oxides has played a significant role in the formation of substantial couplings with SnS precursors, apart from that graphene has also played an important role for their structural growth of the SnS formation. This dual phenomenon has increased the overall electrocatalytic performances, enhanced HER processes with reduced Tafel slopes and low onset overpotentials. Additionally, the long-term stability of the SnS/N-rGO materials across a broader pH range encourages the significant advancements in HER in the near future.^[234] Recently, Dong et al. has synthesized defective MoS₂-rGO based nanoscale materials, which demonstrated exceptional HER performance with a low overpotential of 154 mV, a current density of 10 mA cm⁻², and a modest Tafel slope of 56.17 mV dec⁻¹. The existence of the 1T phase of MoS₂ in the synthesized electrocatalyst may be attributed to the outstanding HER performance of the electrocatalyst. Due to the defect site of the catalyst has opened up new active sites and also accelerate the electrocatalytic processes.

Moreover, the MoS₂ and rGO based nanocomposites can trigger the faster electron transfer kinetics, along with the excellent conductivity and structural stability. As a result, the obtained catalyst exhibited outstanding electrochemical stability.^[235]

7.2. Designing Nanoscale Architecture

Because of the scarcity of conductive channels in the bulk 2D TMDs layers that are present on the conductive substrates, the charge transfer process is quite hindered due to multi-layer sheets of bulk 2D TMDs. Consequently, many nanostructured materials have been developed to facilitate electron transport across the whole electrochemical system, with the goal of improving the catalytic performance of HER catalysts.^[137,236] Constructing an efficient catalyst for electrocatalytic applications on porous conductive substrates for enhanced charge transport. In recent times, monolayer of WS₂,^[237,238] MoS₂,^[239,240] SnS₂,^[241–243] etc.^[244] based nanosheets anchored into the N-doped carbon materials have been synthesized with the help of coaxial spinning strategy. Single layer nanostructures WS₂ attached with the hollow N-doped carbon nanotubes (WS₂@HNCNFs) via simple electrospinning technique were also prepared. The impedance between the layers may be lowered, and the electron transit into the carbon matrix may be improved, as a result of the additional nitrogen doping to the carbon matrix. As expected, the composites assembly along with their good conductivity has shown the enhanced catalytic performances.^[245] This kind of composite materials with excellent conductivity has shown increased electrocatalytic functionality (Figure 12a). Chen et al. investigated the electrical conductivity of MoS₂/MoO₃ based materials by using porous metallic and highly conductive MoO₃ as a base material.^[246] Furthermore, from the 3D porous substrate, Liu et al. created a 2D in plane hybrid

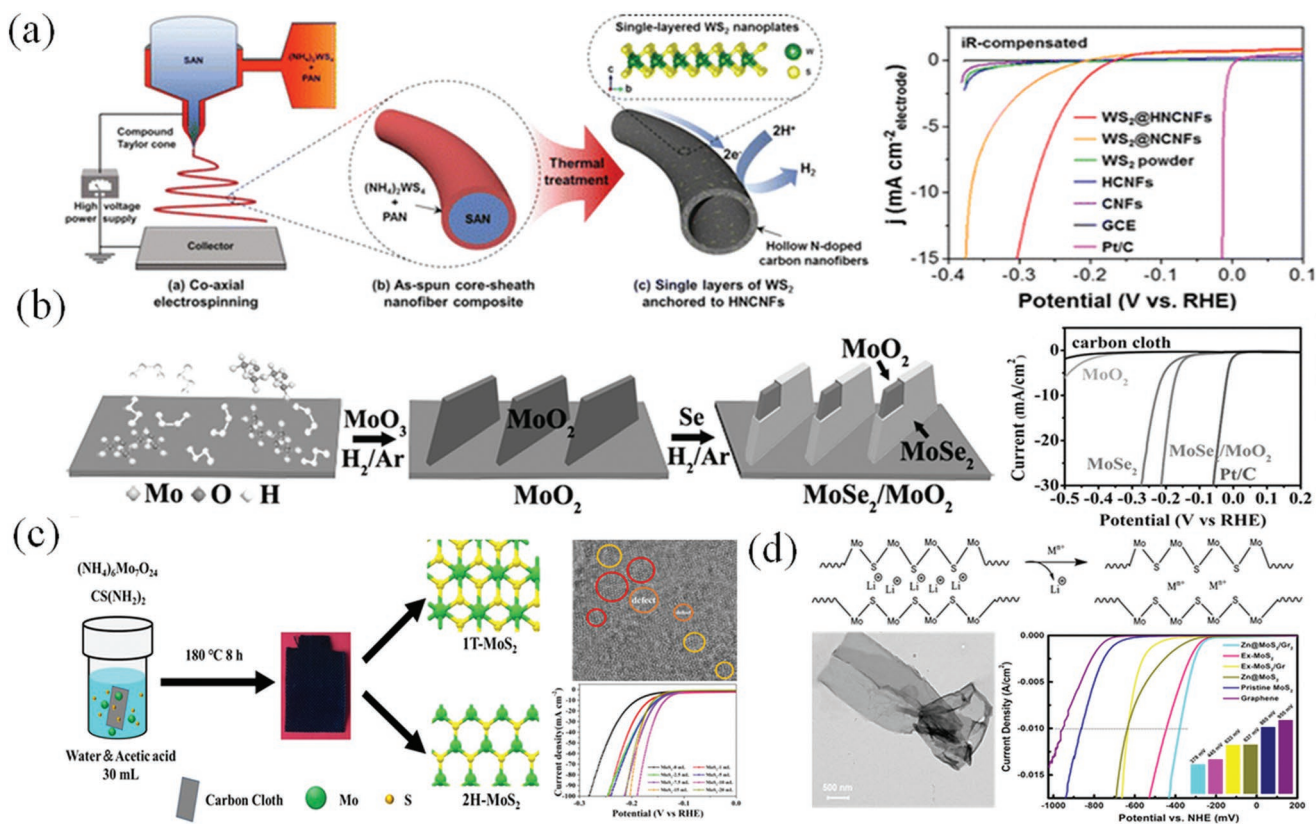


Figure 12. a) Schematic illustration of a,i) coaxial electrospinning, a,ii) as-spun core-sheath SAN@WS₂ precursor/PAN nanofiber composite, which undergoes a subsequent thermal treatment, resulting in a,iii) a core-sheath nanofiber structure where single layers of WS₂ nanoplates are uniformly anchored to hollow N-doped carbon nanofibers and polarization curves (Reproduced with permission.^[224] Copyright 2015, American Chemical Society) b) schematic illustration of the formation of vertical core-shell MoO₃/MoSe₂ nanosheet arrays and polarization curves (Reproduced with permission.^[226] Copyright 2016, Wiley-VCH GmbH) c) schematic of the synthesis of 1T phase-rich MoS₂, TEM images with defect and Polarization curves (Reproduced with permission.^[228] Copyright 2021, American Chemical Society) d) Li₂MoS₄ and metal ion-exchange Method, TEM images of nanosheets and the corresponding polarization curves (Reproduced with permission.^[229] Copyright 2019, American Chemical Society).

nanostructured comprising of small size MoS₂ nanoplates that were homogeneously put into graphene sheets. Within the atomic level basal plane, the in-plane MoS₂-graphene based nanostructures has allowed fast electron transport across the system. The vertically aligned substrate structure may provide adequate conductive pathways and, as a result, allows for the formation of charged nanocrystals on the vertically aligned CNTs, which is advantageous (VA-CNTs). Additionally, it has been shown that vertically stacked quasi-2D based MoO₃/MoSe₂ nanosheets arrays can be formed on more conductive sites.^[247] Due to enhanced crystalline disparity between MoSe₂ and MoO₃ delivered abundant active sites for the hydrogen evolution reactions owing to their increased defects and disorder on the shell. In addition, metallic character of the MoO₃ speed up the overall charge transport for H₂ production in this type of core-shell nanostructure (Figure 12b). Because of the strong synergistic effects of such nanostructures, it has given excellent HER performances. Xu et al. developed low-cost bifunctional catalysts that demonstrated remarkable activity and stability. Using carbon cloth (CC), in-situ fabrication of bifunctional sheet-on-sheet hierarchical MoS₂/NiS₂ heterostructures, which were then further used for water splitting. The MoS₂/NiS₂/CC catalyst has shown high electrochemical performances to hydrogen

evolution reaction (HER) and oxygen evolution reaction (OER), owing to the abundance of heterogeneous interfaces, richness of defects, active sites, and electronic interaction. Exact current densities of 10, 50, and 100 mA cm⁻² can be achieved for HER and OER at overpotentials between 80 and 142 mV, 303 and 348 mV, and 384 and 384 mV, correspondingly. Furthermore, when built as both a cathode and a collector for overall water splitting, a low cell voltage of 1.63 V is needed to obtain a current density of 10 mA cm⁻², suggesting that MoS₂/NiS₂/CC is a good contender for overall water splitting. In a nutshell, this research presents a novel strategy for the further progress of effective bifunctional catalyst for hydrogen production.^[248]

Li et al. has fabricated a defect-rich 1T-MoS₂ nanosheet was created via hydrothermal approach using acetic acid as a templating agent. Increasing or decreasing the quantity of acetic acid may govern the percentage of 1T phase and influence electrocatalytic hydrogen evolution reactions, it has been discovered. The overpotential may be as low as 136 mV at a current density of 10 mA cm⁻² with a Tafel slope of just 45 mV dec⁻¹, indicating a promising future electrocatalytic hydrogen evolution at high concentrations of acetic acid. Using acetic acid as a template, 1T-MoS₂ does not aggregate and as well as

maintains its high conductivity (Figure 12c), paving the way for the creation of long-term stable and low-cost hydrogen evolution reactions in a variety of configurations. Very significantly, the likely method of creation of 1T-MoS₂ nanosheets is given based on a comparison of many tiny molecular carboxylic acid molecules.^[249] Özgür et al. used a straightforward Li exchange technique at a regulated temperature, have created zinc intercalated MoS₂ (Zn@MoS₂) for the first time (Figure 12d). The electrocatalytic activity of Zn@MoS₂ and the synergistic impact of graphene on HER were investigated in 0.5 M H₂SO₄ at room temperature. The Zn@MoS₂ exhibited an overpotential of 0.378 V and a Tafel slope of 81 mV dec⁻¹ with a Tafel slope of 0.378 V. As a consequence of these findings, efficient catalysts for use in water splitting technology is proposed, which has the potential to be applied to the synthesis of additional transition metal-based 2D materials.^[250]

7.3. Coupling Effect in 2D TMDs

The coupling effect between the substrate and the active catalyst has been proved to minimize the contact resistance to a great extent, which directly accelerates the charge transfer kinetics and lower down the hydrogen adsorption energy, i.e., backs up the enhanced HER activity.^[37,248,251] Chhowalla et al. proposed a reaction route for lowering contact resistance between a substrate and active catalysts by the introduction of electronic coupling between the substrate and 2H-MoS₂ nanosheets.^[105] The 2H-MoS₂ nanosheets exhibited excellent HER activity, which has never been previously seen for the intrinsic 2H-MoS₂ nanosheet before this study. The MoS₂ catalysts were loaded with SiO₂ on Si wafers. To ensure excellent conductivity, conductive gold (Au) contacts placed on the MoS₂ nanosheets functioned as electrical contacts, as shown

in Figure 13a. The free electron produced by the dopant may lower the Schottky barrier at the electrical contacts, accelerating charge transfer kinetics between the MoS₂ nanosheets and the conductive substrate. Additionally, the extra electrons in the MoS₂ nanosheet lattice might benefit of the reduction of ΔG_{H^*} . With the decrease in contact resistance, the inert basal plane of the MoS₂ nanosheet may be activated, resulting in a quickening of charge penetration. Moreover, as shown by the polarization curves. (Figure 13), the HER activity improved importantly with the reduction in the contact resistance. With this study, we have discovered a novel method for fabricating large area working electrodes with low contact resistance, which may be used to fully leverage the potential of MoS₂ nanosheets for electrocatalytic hydrogen evolution reaction (HER). From this work, the coupling effect with two or more alternative materials to fabricate nanocomposites can be considered as a powerful way to maximize the advantages and to lower down the disadvantages of the distinct counterpart. Vikraman et al. has successfully synthesized 1T-2H mixed phase MoS₂ on the surface of reduced graphene oxide (rGO) nanocomposites and applied it as efficient electrocatalyst for hydrogen evolution reaction in acidic and alkaline solution. As shown in Figure 13b, the HER findings showed low overpotentials (70 and 71 mV vs RHE), resulting in a current density of 10 mA cm⁻² and modest Tafel slopes (46 and 52 mV dec⁻¹) for 2H-1T MoS₂/rGO hybrid in acidic and alkaline electrolytes, respectively. Chronoamperometric investigations of 2H-1T MoS₂/rGO electrocatalysts in acid and alkaline solutions over 24 h revealed a substantial HER characteristic in both acid and alkaline solutions. In this study, we investigated the fluctuations in the density of states for 2H-1T MoS₂ and rGO hybrid hydrogen adsorbed surfaces using density functional theory (DFT) calculations. The DFT calculation also yielded a low Gibbs energy of 0.01 eV, which confirmed the better experimental HER findings for 2H-1T MoS₂/rGO hybrids.^[252]

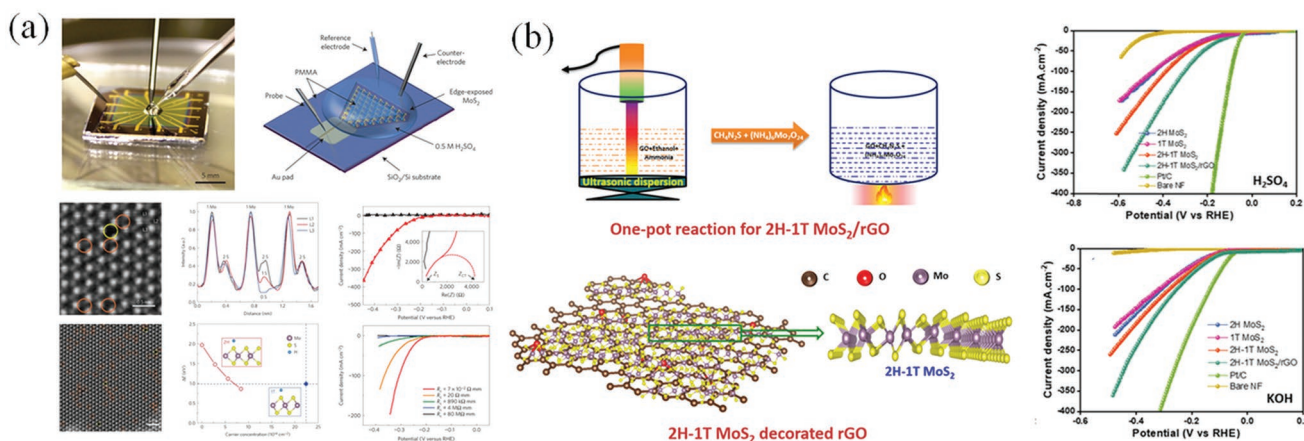


Figure 13. a) Photograph of the electrochemical microcell, schematic of the set-up showing single layer of MoS₂ deposited on SiO₂ and contacted by one gold electrode, STEM image of a single-layer CVD-grown MoS₂ nanosheet with different defects: single sulfur vacancy (orange circle) and double sulfur vacancy (yellow circle), Intensity profiles along lines L1–L3. Higher contrast is obtained from the Mo atoms compared to one sulfur atom (≈30% of the Mo intensity) and two sulfur atoms (≈45% of the Mo intensity). In absence of sulfur atoms (L3), the intensity decreases to <10%, STEM image of a large-area single-layer MoS₂ nanosheet. The vast majority of the defects are formed by single sulfur vacancies. The differential hydrogen adsorption energy (ΔE) in 2H-phase MoS₂ decreases significantly with an increased carrier concentration and their corresponding polarization curves (Reproduced with permission.^[91] Copyright 2016, Nature Publishing Group) b) proposed 2H-1T MoS₂/rGO hybrid creation using one-pot synthesis with ultrasonic dispersion; resulting 2H-1T MoS₂/rGO hybrid structure and their polarization curves (Reproduced with permission.^[231] Copyright 2019, Elsevier).

7.4. Interfacial Engineering

Electrocatalysts based on heterostructure materials with large specific surface have shown substantially faster alkaline and/or acidic HER electrocatalytic kinetics, typically due to the strong synergistic effect from different components, which is playing a key role to control or balance the adsorption/desorption performances of the intermediates at the interfaces. Through various approaches such as interfacial bonding, electrical contact, morphological changes, defects, phases, composition, and lattice strain, interface engineering may successfully enhance the electronic structures of active sites, which might appropriately optimize the binding energy, targeting intermediates such as hydrogen.^[253–258] Xu et al. has successfully demonstrated by potential-temperature depended electrodeposition strategies, we have shown the ultrathin $\text{Ni}(\text{OH})_2/\text{Ni}_3\text{S}_2$ nanosheets (1.8 nm) as a self-assembled nanoforest based electrocatalyst (Figure 14a). When the Ni_3S_2 catalyst is used in conjunction with the $\text{Ni}(\text{OH})_2$ cocatalyst, the surface atomic configuration of Ni_3S_2 is highly regulated, resulting in an efficient acceleration of the different kinetic steps including Volmer step, OH^- adsorption at the time HER process. The electrocatalysis process of the synthesized electrocatalysts to the hydrogen and oxygen evolution reactions in 1 M KOH is superior and steady, with minor overpotentials of 50 mV and 210 mV at 10 mA cm⁻², respectively. An alkaline electrolyzer has used the $\text{Ni}(\text{OH})_2/\text{Ni}_3\text{S}_2$ nanoforest as bi functional catalyst which can make up to 100 mA cm⁻² with minimum cell voltage (1.64 V) even though being stable for 120 h at 1.55 V.^[259] Jia et al. has fabricated the $\text{Mo}_2\text{C}-\text{Mo}_3\text{C}_2$ heteronanowires for high performances HER through interfacial engineering. An accurate phase transition approach is used to fabricate $\text{Mo}_2\text{C}-\text{Mo}_3\text{C}_2$ heteronanowires with

Excellent electrocatalytic results (Figure 14b). The disordering of the structure and the carbon shell on the surface of $\text{Mo}_2\text{C}-\text{Mo}_3\text{C}_2$ heteronanowires has improved surface area and a defect-rich catalytic surface. In addition, the influence of the faulty sites and carbon shell on the free energy for hydrogen adsorption in HER is investigated using theoretical calculations (DFT). For the purpose of improving the HER catalytic performance, it is necessary to assess the synergistic impact between various phases as well as the added lattice defects of $\text{Mo}_2\text{C}-\text{Mo}_3\text{C}_2$. In both acidic and alkaline environments, the proposed catalyst exhibits optimum electrocatalytic activity

with low overpotentials of 134 and 116 mV at 10 mA cm⁻², a modest Tafel slope of 64 mV dec⁻¹, and long-term stability for 5000 cycles. As a result of this experiment, new insights into the design of high-efficiency HER catalysts for commercial water splitting will be gained by interfacial engineering at the nanoscale.^[260] Chen et al. have developed an interface engineering technique that has been shown to be effective in the construction of an efficient and stable catalyst based on $\text{NiS}@\text{MoS}_2$ core-shell hierarchical microspheres. Using in situ growth, ultrathin MoS_2 nanosheets are formed on the surface of NiS hierarchical micro-sized spheres that have been built by porous nanoplates. More crucially, heterostructure formation of MoS_2 nanosheets and NiS nanoplates has helped to adsorption of hydrogen intermediates in a synergistic manner and speeding up the electrocatalytic method for HER. Consequently, the improved $\text{NiS}@\text{MoS}_2$ catalyst exhibits outstanding HER activity and endurance, with a low overpotential of 208 mV in 0.5 M H_2SO_4 and 146 mV in 1.0 M KOH at 10 mA cm⁻², respectively, in the presence of a low overpotential (Figure 14c). The electrocatalytic output confirms that not only the core-shell hierarchical microspheres, but also a multiscale method, are useful in controlling the electronic structure of heterostructure materials for increased hydrogen evolution reaction performance.^[121]

7.5. Effect of Metallic Materials and/or Phase Changes in TMDs

TMDs exhibit a diverse range of physicochemical characteristics, governed by their different crystallographic phase and composition. As an example, in the case of MoS_2 , 2H- MoS_2 is classified as semiconductive materials, although 1T MoS_2 is classified as metallic.^[192,249] The electrocatalytic performances of these two types of MoS_2 in the presence of HER is vastly different. HER can be catalyzed by metallic TMDs, which may be used as competing candidates for catalysis in two different types of MoS_2 , 2H-type MoS_2 has active sites that come exclusively from uncoordinated S atoms at the edges, whereas 1T-type MoS_2 has active sites that originate from the basal surface as well. 1T- MoS_2 is metastable, and intercalation is a process that may be used to achieve phase transition, which results in the creation of 1T- MoS_2 as a result.^[101,152–154,261–264]

In addition, 2D MoS_2 can be found mainly in three phases including 1T (Octahedral symmetry), 2H (Trigonal prismatic

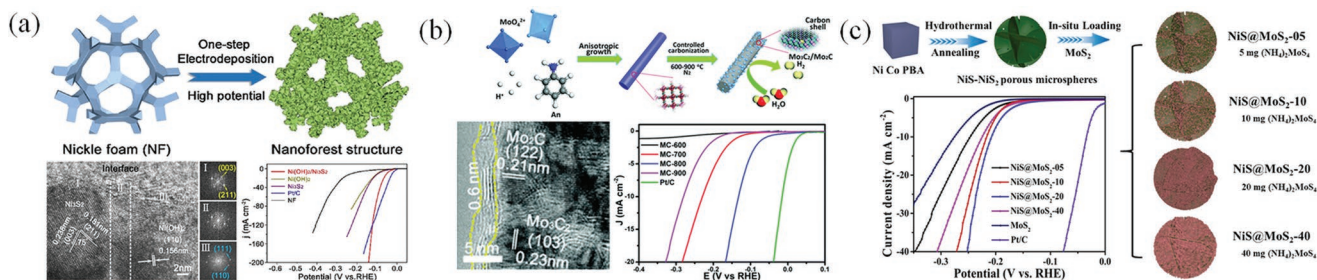


Figure 14. a) Schematic illustration of the electrodeposition synthesis of the nanoforest electrocatalysts, high-resolution TEM image and the selected area FFT patterns and polarisation curves (Reproduced with permission.^[238] Copyright 2019, Elsevier) b) schematic diagrams of the synthetic procedures of the Mo_3C_2 - Mo_2C encapsulated in carbon shell heterostructures, TEM images and their corresponding polarization curves (Reproduced with permission.^[239] Copyright 2019, Royal Society of Chemistry) c) schematic illustration of the formation process of $\text{NiS}@\text{MoS}_2$ core-shell microspheres and corresponding polarization curves (Reproduced with permission.^[107] Copyright 2021, Elsevier).

coordination), and $1T'$ (distorted Octahedral Symmetry). $1T$ MoS_2 is not stable without additional efforts into the S-Mo-S framework, due to its strong aggregation nature and turns into $2H$ MoS_2 owing to their S-S noncovalent interaction. The phase transition can occur between the $1T/1T'$ and $2H$ and/or $2H$ and $1T/1T'$. In $2H$ MoS_2 , the d-orbital splits up into three bands which are $d_{x^2-y^2}$, d_{xy} , d_z^2 , and $d_{xy, xz}$.^[261–263] Hence, it is showing low charge transfer and semiconducting behavior which restricts its application as an electrocatalyst. Whereas the electronic properties of $1T$ MoS_2 has been changed intensively than $2H$ MoS_2 , partially filled $d_{xy, yz, zx}$ orbital generate metallic character in $1T$ MoS_2 phase, which is 10^7 times more conductive compared to $2H$ MoS_2 phase. During electrocatalytic applications, the $1T$ MoS_2 metallic phase removes the Schottky barrier, which enhances the kinetics of charge transfer rate. Due to that, the overpotential and Tafel slope during electrocatalytic hydrogen evolution is much lower in $1T$ MoS_2 compared to $2H$ MoS_2 . However, highly conducting $1T$ - MoS_2 nanosheets obtained through the $2H/1T$ phase transition signifies a more efficient way for further improvement in HER.^[101,261–264]

Jin et al. has fabricated that, $1T$ - MoS_2 nanosheets were formed by simple exfoliation with lithium intercalation from $2H$ - MoS_2 nanostructures that were made on graphite (Figure 15a). Jin and his team found this out in their study.^[194] In addition, the nanosheets of the metallic MoS_2 polymorph demonstrated

simple electrode kinetics and low-loss electrical transport, enabling them to be used as an incredibly competitive earth-abundant high-efficiency HER catalyst (Figure 15b).^[265] In addition, Jiang et al. used DFT calculations to determine the basal plane catalytic activity of $1T$ MoS_2 for improved HER.^[117] It is shown in Figure 15c that the original catalytically inert basal planes are active after phase transition of $2H$ - MoS_2 to $1T$ MoS_2 along with the faster phase transfer from $2H$ MoS_2 to $1T$ MoS_2 . Because of their high affinity for H-atom binding at S edges, the catalytically active basal plane of $1T$ MoS_2 performed much better than the catalytically inert basal plane of $2H$ MoS_2 . With the help of binding free energy using H as the descriptor, they found that the best H_2 evolution proceeded at the surface with 12.5 to 25% H coverage. The whole HER process on the $1T$ MoS_2 basal planes surfaces was given in Figure 14c, from Volmer step, where S atoms of $1T$ MoS_2 adsorbed H atoms with very small barrier of 0.16 eV, surveyed by a Heyrovsky reaction of the H atoms along with the hydronium protons to generate H_2 with an energy barrier of 0.62 eV. Thus, it is proved that the HER occurred easily on the basal planes of $1T$ MoS_2 through Volmer-Heyrovsky mechanism. In addition, few metallic 2D TMDs including TaS, VS_2 , VSe_2 with no bandgaps, manifested excellent HER performances because of their fast charge transfer.^[52,266,267] VS_2 is a typical metallic member of the TMDs family.

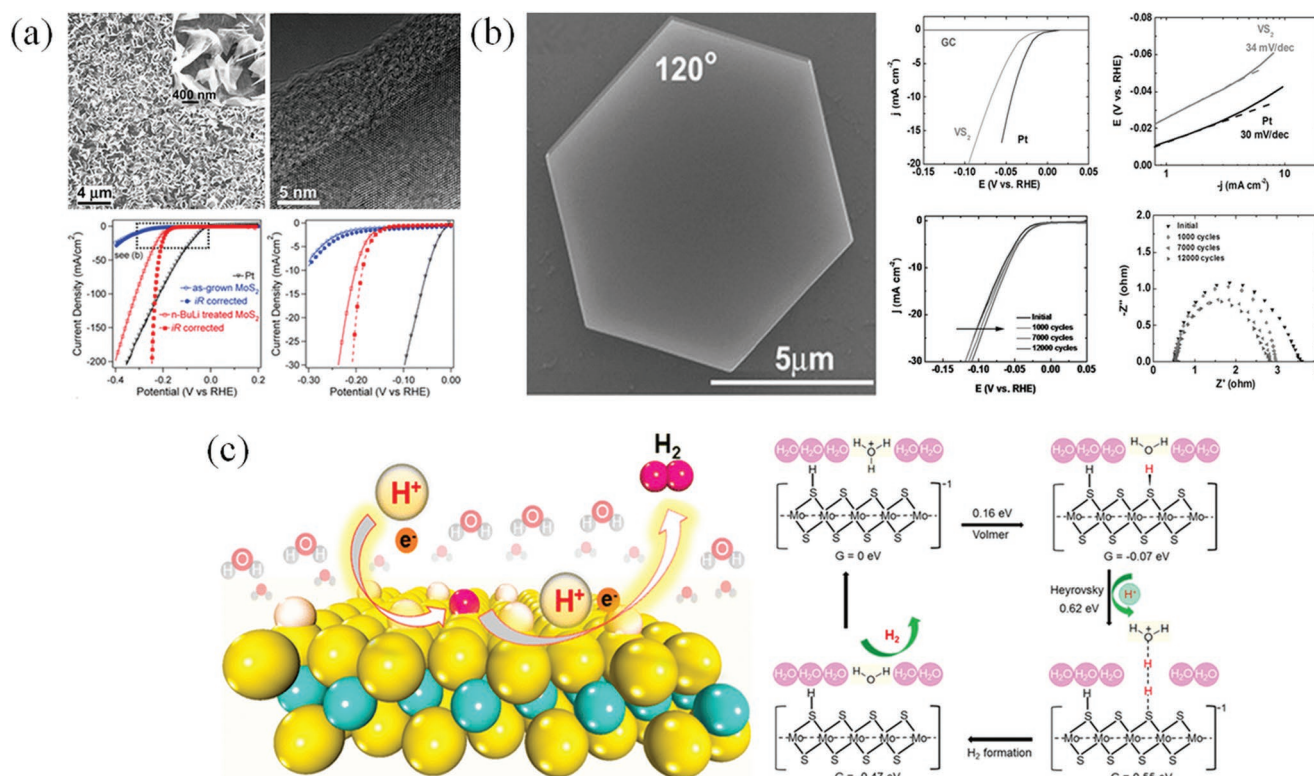


Figure 15. a) Electron microscopy characterization of as-grown $2H$ - MoS_2 nanostructures and their polarization curves (Reproduced with permission.^[240] Copyright 2013, American Chemical Society). b) Scanning electron microscope (SEM) images of VS_2 nanosheets with dominant hexagon and polarization curves after iR -correction, corresponding Tafel plots, polarization curves after various cycles, and Nyquist plots showing that $1T$ - VS_2 maintains excellent catalytic activity after 12,000 cycles of continuous operation (Reproduced with permission.^[242] Copyright 2015, Wiley-VCH GmbH). c) schematic illustration of the MoS_2 surfaces of water splitting for H_2 generation and overall reaction mechanism for HER on the surface of $1T$ MoS_2 . relative free energy (G) values and activation energies (for the Volmer and Heyrovsky steps) (Reproduced with permission.^[103] Copyright 2016, American Chemical Society).

Table 2. Advantage and disadvantage of the different fabrication process.

Advantages and disadvantages of the different fabrication processes		
Synthetic Strategy	Advantages	Disadvantages
Chemical Vapor Deposition	<ul style="list-style-type: none"> • Heterostructure formation • Interfacial engineering • Efficient 2D nanostructures • Highly selective 	<ul style="list-style-type: none"> • Expensive Instruments • High Temperature • Limited synthesis • Low yield
Hydro-Solvothermal Method	<ul style="list-style-type: none"> • Controlled morphology • Well dispersion rate • Efficient and Selective • Less expensive 	<ul style="list-style-type: none"> • Complex reaction mechanism • Template assisted method • Time consuming
Solid State synthesis	<ul style="list-style-type: none"> • Less expensive • Simple and fast process • High yield 	<ul style="list-style-type: none"> • Low quality morphology • Less purity • Low catalytic activity
Hot injection strategy	<ul style="list-style-type: none"> • Uniform morphology and Size • Highly Crystalline • Less time consuming 	<ul style="list-style-type: none"> • Low yield • Depletion of organic molecule on the materials surface
Colloidal synthesis	<ul style="list-style-type: none"> • Quality of materials • Wide scale size and morphology • Wide scale materials 	<ul style="list-style-type: none"> • Complex reaction procedure • Using organic ligand • Difficult to separate from catalytic system • Low yield

Lou et al. demonstrated a simple CVD approach for synthesizing VS₂ single crystal nanosheets, as seen in Figure 15c. The resistivity of VS₂ decreased as the temperature decreased, as seen in Figure 13d, indicating its inherent metallic nature. The 1T-VS₂ crystals demonstrated excellent electrocatalytic activity for HER, with an exceptionally low overpotential (68 mV) at a current density of 10 mA cm⁻², modest Tafel slopes (34 mV dec⁻¹) (Figure 15b), and remarkable stability over long time. Electrochemical impedance spectroscopy (EIS) investigations were used to determine the charge transfer efficiency. Due to minimum charge transfer resistance of 3U for 1T-VS₂, which is signifying the catalyst potential as a potential non noble based electrocatalyst for HER (Table 2).^[267]

The most important physicochemical properties of 2D transition metal chalcogenides have been benefited by their activated basal plane, edges, strain, controlled morphology, and monolayers, which are helping them to build excellent electrocatalytic materials for HER.^[42–44,113,268] Generally, metal chalcogenides have been fabricated through different synthetic strategies including CVD, hydrothermal colloidal, solid states, etc., which have been discussed in earlier sections and shown in Table 1. 2D metal chalcogenide-based materials in various forms are very important nanostructures for the electrocatalytic performances of hydrogen evolution reactions toward a greener environment.^[113,268–270]

8. Conclusions

In this review, it is discussed the current development and their future research in transition metal dichalcogenide (TMDs) area. Our main target was to explore in the basic concepts, synthesis, and details discussion of 2D TMDs encompassing their different catalytic activities. The main advantages of the 2D plane with most exposed active sites and their fast diffusion

path confirms the enhanced catalytic performances, which is equivalent to the expensive Pt based electrocatalyst. However, owing to their presence of different atomic arrangement and chemical accessibility of the nanoscale 2D TMDs materials. Additionally, it is also possible to increase their catalytic activity further by the alter of synthetic strategies which lead to the results of different potential electrocatalytic results. In general, different features are being followed including engineering the 2D nanomaterials, edge and strain engineering, creating defect, heteroatom doping, metallic materials, fabrication of nanocomposites multilayer to single layers, and enhancement of their overall charge transfer for creating more effective sites for HER. From these different physicochemical properties of the 2D TMDs for highly performed HER electrocatalyst. Though, excellent activity has been made in a good direction as well as more workable or effective materials need to be developed. The key drawback of the HER process via electrocatalysis is deterioration of the catalysis during long term catalysis, owing to that more efficient and less corrosive catalyst need to be explored in near future. The corresponding HER mechanism of the 2D materials are still not clear and need further investigation. From these points of view, research investigation on the 2D materials at nanoscale level simplify the future industrial relevant applications.

Acknowledgements

The authors acknowledge the Kempe Foundation, the Knut och Alice Wallenberg Foundation, and the Luleå University of Technology for financial support.

Conflict of Interest

The authors declare no conflict of interest.

Keywords

2D materials, electrocatalyses, hydrogen evolution reactions, transition metal dichalcogenides

Received: August 4, 2022

Revised: September 20, 2022

Published online: October 30, 2022

- [1] S. H. Mohr, J. Wang, G. Ellem, J. Ward, D. Giurco, *Fuel* **2015**, 141, 120.
- [2] S. Prasad, V. Venkatramanan, A. Singh, in *Sustainable Bioeconomy*, Springer, Singapore **2021**, 267–284.
- [3] H. S. Boudet, *Nat. Energy* **2019**, 4, 446.
- [4] K. T. Möller, T. R. Jensen, E. Akiba, H. Li, *Prog. Nat. Sci. Mater. Int.* **2017**, 27, 34.
- [5] A. Züttel, A. Remhof, A. Borgschulte, O. Friedrichs, *Philos. Trans. R. Soc. A* **2010**, 368, 3329.
- [6] R. P. Drake, *High Energy Density Phys.* **2018**, 1.
- [7] R. Ramachandran, *Int. J. Hydrogen Energy* **1998**, 23, 593.
- [8] S. Atilhan, S. Park, M. M. El-Halwagi, M. Atilhan, M. Moore, R. B. Nielsen, *Curr. Opin. Chem. Eng.* **2021**, 31, 100668.
- [9] Y. Chen, H. Zuo, *Ironmaking Steelmaking* **2021**, 48, 749.
- [10] J. Qi, W. Zhang, R. Cao, *Adv. Energy Mater.* **2018**, 8, 1701620.
- [11] J. E. Mason, *Energy Policy* **2007**, 35, 1315.
- [12] N. Sazali, *Int. J. Hydrogen Energy* **2020**, 45, 18753.
- [13] B. Widera, *Therm. Sci. Eng. Prog.* **2020**, 16, 100460.
- [14] N. V. Gnanapragasam, B. V. Reddy, M. A. Rosen, *Int. J. Hydrogen Energy* **2010**, 35, 4933.
- [15] D. L. Stojić, M. P. Marčeta, S. P. Sovilj, Š. S. Miljanić, *J. Power Sources* **2003**, 118, 115.
- [16] C. N. Ávila-Neto, S. C. Dantas, F. A. Silva, T. V. Franco, L. L. Romanielo, C. E. Hori, A. J. Assis, *J. Nat. Gas Sci. Eng.* **2009**, 1, 205.
- [17] X. Zou, Y. Zhang, *Chem. Soc. Rev.* **2015**, 44, 5148.
- [18] M. Grätzel, *Nature* **2001**, 414, 338.
- [19] S. Wang, A. Lu, C.-J. Zhong, *Nano Convergence* **2021**, 8, 4.
- [20] Y. Kuang, G. Feng, P. Li, Y. Bi, Y. Li, X. Sun, *Angew. Chem.* **2016**, 128, 703.
- [21] I. Concina, Z. H. Ibupoto, A. Vomiero, *Adv. Energy Mater.* **2017**, 7, 1770138.
- [22] A. Mondal, A. Paul, D. N. Srivastava, A. B. Panda, *Int. J. Hydrogen Energy* **2018**, 43, 21665.
- [23] J. McAllister, N. A. G. Bandeira, J. C. McGlynn, A. Y. Ganin, Y.-F. Song, C. Bo, H. N. Miras, *Nat. Commun.* **2019**, 10, 370.
- [24] G. Solomon, R. Mazzaro, V. Morandi, I. Concina, A. Vomiero, *Crystals* **2020**, 10, 1040.
- [25] A. Mondal, K. Sinha, A. Paul, D. N. Srivastava, A. B. Panda, *Int. J. Hydrogen Energy* **2020**, 45, 18623.
- [26] L. Yu, S. Song, B. McElhenny, F. Ding, D. Luo, Y. Yu, S. Chen, Z. Ren, *J. Mater. Chem. A* **2019**, 7, 19728.
- [27] H. Du, R.-M. Kong, X. Guo, F. Qu, J. Li, *Nanoscale* **2018**, 10, 21617.
- [28] R. Wang, J. Huang, X. Zhang, J. Han, Z. Zhang, T. Gao, L. Xu, S. Liu, P. Xu, B. Song, *ACS Nano* **2022**, 16, 3593.
- [29] X. Xia, L. Wang, N. Sui, V. L. Colvin, W. W. Yu, *Nanoscale* **2020**, 12, 12249.
- [30] S. A. Han, R. Bhatia, S.-W. Kim, *Nano Convergence* **2015**, 2, 17.
- [31] W. Choi, N. Choudhary, G. H. Han, J. Park, D. Akinwande, Y. H. Lee, *Mater. Today* **2017**, 20, 116.
- [32] H. Wang, H. Yuan, S. Sae Hong, Y. Li, Y. Cui, *Chem. Soc. Rev.* **2015**, 44, 2664.
- [33] Y. Qu, H. Pan, C. T. Kwok, *Sci. Rep.* **2016**, 6, 34186.
- [34] X. Li, X. Wu, *Wiley Interdiscip. Rev. Comput. Mol. Sci.* **2016**, 6, 441.
- [35] H. G. Ji, P. Solís-Fernández, U. Erkiş, H. Ago, *ACS Appl. Nano Mater.* **2021**, 4, 3717.
- [36] M. Deng, X. Wang, J. Chen, Z. Li, M. Xue, Z. Zhou, F. Lin, X. Zhu, Z. Fang, *Adv. Funct. Mater.* **2021**, 31, 2010234.
- [37] D. Voire, J. Yang, M. Chhowalla, *Adv. Mater.* **2016**, 28, 6197.
- [38] X. Cao, C. Tan, X. Zhang, W. Zhao, H. Zhang, *Adv. Mater.* **2016**, 28, 6167.
- [39] Q. Yu, Y. Luo, A. Mahmood, B. Liu, H.-M. Cheng, *Electrochem. Energy Rev.* **2019**, 2, 373.
- [40] Z. Liu, T. He, Q. Jiang, W. Wang, J. Tang, *Int. J. Hydrogen Energy* **2022**, 47, 29698.
- [41] T. Tang, Z. Wang, J. Guan, *Chin. J. Catal.* **2022**, 43, 636.
- [42] P. Sundara Venkatesh, N. Kannan, M. Ganesh Babu, G. Paulraj, K. Jeganathan, *Int. J. Hydrogen Energy* **2022**, 47, 35123.
- [43] Y. Sim, Y. Chae, S.-Y. Kwon, *iScience* **2022**, 105098.
- [44] S. Li, B. Fei, *Mater. Sci. Technol.* **2022**, 38, 535.
- [45] Z. Wang, M. T. Tang, A. Cao, K. Chan, J. K. Nørskov, *J. Phys. Chem. C* **2022**, 126, 5151.
- [46] A. Y. Ganin, M. D. Symes, *Curr. Opin. Electrochem.* **2022**, 34, 101001.
- [47] P. Zhang, H. Xiang, L. Tao, H. Dong, Y. Zhou, T. S. Hu, X. Chen, S. Liu, S. Wang, S. Garaj, *Nano Energy* **2019**, 57, 535.
- [48] S. Anantharaj, S. Noda, in *Sulfide and Selenide Based Materials for Emerging Applications*, Elsevier, New York **2022**, 495–525.
- [49] H. G. Shiraz, X. Crispin, M. Berggren, *Int. J. Hydrogen Energy* **2021**, 46, 24060.
- [50] L. Lin, P. Sherrell, Y. Liu, W. Lei, S. Zhang, H. Zhang, G. G. Wallace, J. Chen, *Adv. Energy Mater.* **2020**, 10, 1903870.
- [51] C. Xu, S. Peng, C. Tan, H. Ang, H. Tan, H. Zhang, Q. Yan, *J. Mater. Chem. A* **2014**, 2, 5597.
- [52] H. Li, Y. Tan, P. Liu, C. Guo, M. Luo, J. Han, T. Lin, F. Huang, M. Chen, *Adv. Mater.* **2016**, 28, 8945.
- [53] G. Ye, Y. Gong, J. Lin, B. Li, Y. He, S. T. Pantelides, W. Zhou, R. Vajtai, P. M. Ajayan, *Nano Lett.* **2016**, 16, 1097.
- [54] L. Tao, X. Duan, C. Wang, X. Duan, S. Wang, *Chem. Commun.* **2015**, 51, 7470.
- [55] R. J. Smith, P. J. King, M. Lotya, C. Wirtz, U. Khan, S. De, A. O'Neill, G. S. Duesberg, J. C. Grunlan, G. Moriarty, J. Chen, J. Wang, A. I. Minett, V. Nicolosi, J. N. Coleman, *Adv. Mater.* **2011**, 23, 3944.
- [56] Y.-H. Lee, X.-Q. Zhang, W. Zhang, M.-T. Chang, C.-T. Lin, K.-D. Chang, Y.-C. Yu, J. T.-W. Wang, C.-S. Chang, L.-J. Li, T.-W. Lin, *Adv. Mater.* **2012**, 24, 2320.
- [57] K.-K. Liu, W. Zhang, Y.-H. Lee, Y.-C. Lin, M.-T. Chang, C.-Y. Su, C.-S. Chang, H. Li, Y. Shi, H. Zhang, C.-S. Lai, L.-J. Li, *Nano Lett.* **2012**, 12, 1538.
- [58] Y. Yu, S.-Y. Huang, Y. Li, S. N. Steinmann, W. Yang, L. Cao, *Nano Lett.* **2014**, 14, 553.
- [59] A. Mondal, A. Paul, D. N. Srivastava, A. B. Panda, *ACS Appl. Nano Mater.* **2018**, 1, 4622.
- [60] X. Huang, M. Leng, W. Xiao, M. Li, J. Ding, T. L. Tan, W. S. V. Lee, J. Xue, *Adv. Funct. Mater.* **2017**, 27, 1604943.
- [61] S. Chandrasekaran, D. Ma, Y. Ge, L. Deng, C. Bowen, J. Roscow, Y. Zhang, Z. Lin, R. D. K. Misra, J. Li, P. Zhang, H. Zhang, *Nano Energy* **2020**, 77, 105080.
- [62] J. Lee, C. Kim, K. Choi, J. Seo, Y. Choi, W. Choi, Y.-M. Kim, H. Y. Jeong, J. H. Lee, G. Kim, H. Park, *Nano Energy* **2019**, 63, 103846.
- [63] H. Jin, X. Liu, S. Chen, A. Vasileff, L. Li, Y. Jiao, L. Song, Y. Zheng, S.-Z. Qiao, *ACS Energy Lett.* **2019**, 4, 805.
- [64] A. VahidMohammadi, J. Rosen, Y. Gogotsi, *Science* **2021**, 372, abf1581.
- [65] J. Fu, R. Ali, C. Mu, Y. Liu, N. Mahmood, W.-M. Lau, X. Jian, *Chem. Eng. J.* **2021**, 411, 128494.
- [66] B. A. Yusuf, M. Xie, N. Ullah, C. J. Oluigbo, W. Yaseen, J. Xie, Y. Xu, *Appl. Surf. Sci.* **2021**, 537, 147971.

- [67] D. Vikraman, S. Hussain, S. A. Patil, L. Truong, A. A. Arbab, S. H. Jeong, S.-H. Chun, J. Jung, H.-S. Kim, *ACS Appl. Mater. Interfaces* **2021**, 13, 5061.
- [68] L. Li, X. Wang, J. Li, Y. Guo, X. Li, Y. Lu, *J. Alloys Compd.* **2021**, 872, 159562.
- [69] Y. Xu, R. Wang, J. Wang, J. Li, T. Jiao, Z. Liu, *Chem. Eng. J.* **2021**, 417, 129233.
- [70] Z. H. Ibupoto, A. Tahira, P. Tang, X. Liu, J. R. Morante, M. Fahlman, J. Arbiol, M. Vagin, A. Vomiero, *Adv. Funct. Mater.* **2019**, 29, 1807562.
- [71] A. Tahira, Z. H. Ibupoto, R. Mazzaro, S. You, V. Morandi, M. M. Natile, M. Vagin, A. Vomiero, *ACS Appl. Energy Mater.* **2019**, 2, 2053.
- [72] G. Solomon, R. Mazzaro, S. You, M. M. Natile, V. Morandi, I. Concina, A. Vomiero, *ACS Appl. Mater. Interfaces* **2019**, 11, 22380.
- [73] S. P. Kaur, T. J. Dhillip Kumar, *Appl. Surf. Sci.* **2021**, 552, 149146.
- [74] Q. Ji, Y. Zhang, Y. Zhang, Z. Liu, *Chem. Soc. Rev.* **2015**, 44, 2587.
- [75] D. Liu, G. Pang, Z. Tang, S. Feng, *Inorg. Chem. Front.* **2019**, 6, 2043.
- [76] L.-C. Tang, L. Zhao, L.-Z. Guan, in *Advanced Composite Materials: Properties and Applications*, De Gruyter Open, Berlin, Germany **2017**, p. 349–419.
- [77] S. Wang, M. S. Ukhtary, R. Saito, *Phys. Rev. Res.* **2020**, 2, 033340.
- [78] Y. Chen, K. Yang, B. Jiang, J. Li, M. Zeng, L. Fu, *J. Mater. Chem. A* **2017**, 5, 8187.
- [79] N. Dubouis, A. Grimaud, *Chem. Sci.* **2019**, 10, 9165.
- [80] Y. Zheng, Y. Jiao, A. Vasileff, S. Qiao, *Angew. Chem. Int. Ed.* **2018**, 57, 7568.
- [81] J. Kim, H. Kim, W.-J. Lee, B. Ruqia, H. Baik, H.-S. Oh, S.-M. Paek, H.-K. Lim, C. H. Choi, S.-I. Choi, *J. Am. Chem. Soc.* **2019**, 141, 18256.
- [82] M. Đurovič, J. Hnát, K. Bouzek, *J. Power Sources* **2021**, 493, 229708.
- [83] S. Jayabal, G. Saranya, J. Wu, Y. Liu, D. Geng, X. Meng, *J. Mater. Chem. A* **2017**, 5, 24540.
- [84] M. Tavares, S. A. Machado, L. Mazo, *Electrochim. Acta* **2001**, 46, 4359.
- [85] S. Watzele, J. Fichtner, B. Garlyyev, J. N. Schwämmlein, A. S. Bandarenka, *ACS Catal.* **2018**, 8, 9456.
- [86] B. Hinnemann, P. G. Moses, J. Bonde, K. P. Jørgensen, J. H. Nielsen, S. Hørch, I. Chorkendorff, J. K. Nørskov, *J. Am. Chem. Soc.* **2005**, 127, 5308.
- [87] Y. M. Hao, H. Nakajima, A. Inada, K. Sasaki, K. Ito, *Electrochim. Acta* **2019**, 301, 274.
- [88] M. R. G. de Chialvo, A. C. Chialvo, *J. Electroanal. Chem.* **1994**, 372, 209.
- [89] J. K. Nørskov, T. Bligaard, A. Logadottir, J. R. Kitchin, J. G. Chen, S. Pandalov, U. Stimming, *J. Electrochem. Soc.* **2005**, 152, 123.
- [90] A. B. Laursen, A. S. Varela, F. Dionigi, H. Fanchiu, C. Miller, O. L. Trinhammer, J. Rossmeisl, S. Dahl, *J. Chem. Educ.* **2012**, 89, 1595.
- [91] E. Pomerantseva, C. Resini, K. Kovnir, Y. V. Kolen'ko, *Adv. Phys. X* **2017**, 2, 211.
- [92] Z. W. Seh, J. Kibsgaard, C. F. Dickens, I. Chorkendorff, J. K. Nørskov, T. F. Jaramillo, *Science* **2017**, 355, aad4998.
- [93] B. E. Conway, B. V. Tilak, *Electrochim. Acta* **2002**, 47, 3571.
- [94] T. Shinagawa, A. T. Garcia-Esparza, K. Takanabe, *Sci. Rep.* **2015**, 5, 13801.
- [95] B. Subramanya, Y. Ullal, S. U. Shenoy, D. K. Bhat, A. C. Hegde, *RSC Adv.* **2015**, 5, 47398.
- [96] D. Chanda, J. Hnát, A. S. Dobrota, I. A. Pašti, M. Paidar, K. Bouzek, *Phys. Chem. Chem. Phys.* **2015**, 17, 26864.
- [97] R. S. Situmorang, O. Seri, H. Kawai, *Appl. Surf. Sci.* **2020**, 505, 144300.
- [98] J. Yu, Q. He, G. Yang, W. Zhou, Z. Shao, M. Ni, *ACS Catal.* **2019**, 9, 9973.
- [99] C. G. Morales-Guio, L.-A. Stern, X. Hu, *Chem. Soc. Rev.* **2014**, 43, 6555.
- [100] B. Yu, F. Qi, Y. Chen, X. Wang, B. Zheng, W. Zhang, Y. Li, L.-C. Zhang, *ACS Appl. Mater. Interfaces* **2017**, 9, 30703.
- [101] J. Xie, J. Zhang, S. Li, F. Grote, X. Zhang, H. Zhang, R. Wang, Y. Lei, B. Pan, Y. Xie, *J. Am. Chem. Soc.* **2013**, 135, 17881.
- [102] A. Jiang, B. Zhang, Z. Li, G. Jin, J. Hao, *Chem. Asian J.* **2018**, 13, 1438.
- [103] H. Li, C. Tsai, A. L. Koh, L. Cai, A. W. Contryman, A. H. Fragapane, J. Zhao, H. S. Han, H. C. Manoharan, F. Abild-Pedersen, J. K. Nørskov, X. Zheng, *Nat. Mater.* **2016**, 15, 48.
- [104] I. S. Kwon, I. H. Kwak, J. Y. Kim, T. T. Debela, Y. C. Park, J. Park, H. S. Kang, *ACS Nano* **2021**, 15, 5467.
- [105] D. Voiry, R. Fullon, J. Yang, C. de Carvalho Castro e Silva, R. Kappera, I. Bozkurt, D. Kaplan, M. J. Lagos, P. E. Batson, G. Gupta, A. D. Mohite, L. Dong, D. Er, V. B. Shenoy, T. Asefa, M. Chhowalla, *Nat. Mater.* **2016**, 15, 1003.
- [106] H. R. Inta, S. Ghosh, A. Mondal, G. Tudu, H. V. S. R. M. Koppiseti, V. Mahalingam, *ACS Appl. Energy Mater.* **2021**, 4, 2828.
- [107] J. Shi, D. Ma, G.-F. Han, Y. Zhang, Q. Ji, T. Gao, J. Sun, X. Song, C. Li, Y. Zhang, X.-Y. Lang, Y. Zhang, Z. Liu, *ACS Nano* **2014**, 8, 10196.
- [108] Z. Wu, B. Fang, Z. Wang, C. Wang, Z. Liu, F. Liu, W. Wang, A. Alfantazi, D. Wang, D. P. Wilkinson, *ACS Catal.* **2013**, 3, 2101.
- [109] Y. Yan, S. Xu, H. Li, N. C. S. Selvam, J. Y. Lee, H. Lee, P. J. Yoo, *Chem. Eng. J.* **2021**, 405, 126728.
- [110] Y. Tan, P. Liu, L. Chen, W. Cong, Y. Ito, J. Han, X. Guo, Z. Tang, T. Fujita, A. Hirata, M. W. Chen, *Adv. Mater.* **2014**, 26, 8023.
- [111] N. Xie, D.-D. Ma, Y.-L. Wu, X.-T. Wu, Q.-L. Zhu, *Sustainable Energy Fuels* **2021**, 5, 2633.
- [112] Y. Zhang, Q. Ji, G.-F. Han, J. Ju, J. Shi, D. Ma, J. Sun, Y. Zhang, M. Li, X.-Y. Lang, Y. Zhang, Z. Liu, *ACS Nano* **2014**, 8, 8617.
- [113] Y. Yin, J. Han, Y. Zhang, X. Zhang, P. Xu, Q. Yuan, L. Samad, X. Wang, Y. Wang, Z. Zhang, P. Zhang, X. Cao, B. Song, S. Jin, *J. Am. Chem. Soc.* **2016**, 138, 7965.
- [114] J. Mujtaba, L. He, H. Zhu, Z. Xiao, G. Huang, A. A. Solovev, Y. Mei, *ACS Appl. Nano Mater.* **2021**, 4, 1776.
- [115] D. McAteer, Z. Gholamvand, N. McEvoy, A. Harvey, E. O'Malley, G. S. Duesberg, J. N. Coleman, *ACS Nano* **2016**, 10, 672.
- [116] Z. Zhang, W. Li, M. F. Yuen, T.-W. Ng, Y. Tang, C.-S. Lee, X. Chen, W. Zhang, *Nano Energy* **2015**, 18, 196.
- [117] Q. Tang, D. Jiang, *ACS Catal.* **2016**, 6, 4953.
- [118] S. Pan, S. Ma, C. Chang, X. Long, K. Qu, Z. Yang, *Mater. Today Phys.* **2021**, 18, 100401.
- [119] X. Sun, J. Dai, Y. Guo, C. Wu, F. Hu, J. Zhao, X. Zeng, Y. Xie, *Nanoscale* **2014**, 6, 8359.
- [120] B. Seo, G. Y. Jung, Y. J. Sa, H. Y. Jeong, J. Y. Cheon, J. H. Lee, H. Y. Kim, J. C. Kim, H. S. Shin, S. K. Kwak, S. H. Joo, *ACS Nano* **2015**, 9, 3728.
- [121] Z. Chen, X. Liu, P. Xin, H. Wang, Y. Wu, C. Gao, Q. He, Y. Jiang, Z. Hu, S. Huang, *J. Alloys Compd.* **2021**, 853, 157352.
- [122] Y. Zhang, L. Zuo, Y. Huang, L. Zhang, F. Lai, W. Fan, T. Liu, *ACS Sustainable Chem. Eng.* **2015**, 3, 3140.
- [123] Y. Liu, H. Li, J. Li, X. Ma, Z. Cui, D. Gao, Z. Tang, *J. Mater. Chem. A* **2021**, 9, 14451.
- [124] X. Chia, A. Ambrosi, P. Lazar, Z. Sofer, M. Pumera, *J. Mater. Chem. A* **2016**, 4, 14241.
- [125] S. Y. Shajaripour Jaber, A. Ghaffarinejad, Z. Khajehsaeidi, *Int. J. Hydrogen Energy* **2021**, 46, 3922.
- [126] M. S. Faber, M. A. Lukowski, Q. Ding, N. S. Kaiser, S. Jin, *J. Phys. Chem. C* **2014**, 118, 21347.
- [127] Y. Xiao, M. Tan, Z. Li, L. He, B. Gao, Y. Chen, Y. Zheng, B. Lin, *Int. J. Hydrogen Energy* **2021**, 46, 11688.
- [128] W. Zhao, B. Dong, Z. Guo, G. Su, R. Gao, W. Wang, L. Cao, *Chem. Commun.* **2016**, 52, 9228.
- [129] Y. Zhang, L. Zuo, L. Zhang, Y. Huang, H. Lu, W. Fan, T. Liu, *ACS Appl. Mater. Interfaces* **2016**, 8, 7077.

- [130] B. Zhou, J. Li, X. Zhang, J. Guo, *J. Alloys Compd.* **2021**, 862, 158391.
- [131] A. K. Nayak, E. Enhtuwshin, S. J. Kim, H. Han, *Catalysts* **2020**, 10, 1238.
- [132] L. Najafi, S. Bellani, R. Oropesa-Nuñez, B. Martín-García, M. Prato, L. Pasquale, J.-K. Panda, P. Marvan, Z. Sofer, F. Bonaccorso, *ACS Catal.* **2020**, 10, 3313.
- [133] H. Huang, J. Song, D. Yu, Y. Hao, Y. Wang, S. Peng, *Appl. Surf. Sci.* **2020**, 525, 146623.
- [134] B. Qu, C. Li, C. Zhu, S. Wang, X. Zhang, Y. Chen, *Nanoscale* **2016**, 8, 16886.
- [135] H. Tang, K. Dou, C.-C. Kaun, Q. Kuang, S. Yang, *J. Mater. Chem. A* **2014**, 2, 360.
- [136] M. D. Sharma, C. Mahala, M. Basu, *Inorg. Chem.* **2020**, 59, 4377.
- [137] B. Qu, X. Yu, Y. Chen, C. Zhu, C. Li, Z. Yin, X. Zhang, *ACS Appl. Mater. Interfaces* **2015**, 7, 14170.
- [138] Z. Lei, S. Xu, P. Wu, *Phys. Chem. Chem. Phys.* **2016**, 18, 70.
- [139] K. Karupphasamy, R. Bose, V. R. Jothi, D. Vikraman, Y.-T. Jeong, P. Arunkumar, D. B. Velusamy, T. Maiyalagan, A. Alfantazi, H.-S. Kim, *J. Alloys Compd.* **2020**, 838, 155537.
- [140] H. Wang, D. Kong, P. Johanes, J. J. Cha, G. Zheng, K. Yan, N. Liu, Y. Cui, *Nano Lett.* **2013**, 13, 3426.
- [141] R. Wang, Q. Shao, Q. Yuan, P. Sun, R. Nie, X. Wang, *Appl. Surf. Sci.* **2020**, 504, 144320.
- [142] Y. Li, X. Yin, X. Huang, X. Liu, W. Wu, *Int. J. Hydrogen Energy* **2020**, 45, 16489.
- [143] C. Liu, K. Wang, X. Zheng, X. Liu, Q. Liang, Z. Chen, *Carbon* **2018**, 139, 1.
- [144] J. Zhang, T. Wang, D. Pohl, B. Rellinghaus, R. Dong, S. Liu, X. Zhuang, X. Feng, *Angew. Chem.* **2016**, 128, 6814.
- [145] D. Vikraman, S. Hussain, K. Akbar, L. Truong, A. Kathalingam, S.-H. Chun, J. Jung, H. J. Park, H.-S. Kim, *ACS Sustainable Chem. Eng.* **2018**, 6, 8400.
- [146] Y. Guo, J. Tang, H. Qian, Z. Wang, Y. Yamauchi, *Chem. Mater.* **2017**, 29, 5566.
- [147] X.-Y. Yu, H. Hu, Y. Wang, H. Chen, X. W. D. Lou, *Angew. Chem.* **2015**, 127, 7503.
- [148] X. Xu, Y. Ge, M. Wang, Z. Zhang, P. Dong, R. Baines, M. Ye, J. Shen, *ACS Appl. Mater. Interfaces* **2016**, 8, 18036.
- [149] R. D. Nikam, A.-Y. Lu, P. A. Sonawane, U. R. Kumar, K. Yadav, L.-J. Li, Y.-T. Chen, *ACS Appl. Mater. Interfaces* **2015**, 7, 23328.
- [150] Y. Liu, X. Hua, C. Xiao, T. Zhou, P. Huang, Z. Guo, B. Pan, Y. Xie, *J. Am. Chem. Soc.* **2016**, 138, 5087.
- [151] G. Zhao, P. Li, K. Rui, Y. Chen, S. X. Dou, W. Sun, *Chem. Eur. J.* **2018**, 24, 11158.
- [152] G. Zhao, K. Rui, S. X. Dou, W. Sun, *Adv. Funct. Mater.* **2018**, 28, 1803291.
- [153] G. Shao, X. Xue, B. Wu, Y. Lin, M. Ouzounian, T. S. Hu, Y. Xu, X. Liu, S. Li, K. Suenaga, Y. Feng, S. Liu, *Adv. Funct. Mater.* **2020**, 30, 1906069.
- [154] X. Geng, W. Wu, N. Li, W. Sun, J. Armstrong, A. Al-hilo, M. Brozak, J. Cui, T. Chen, *Adv. Funct. Mater.* **2014**, 24, 6123.
- [155] Z. Lin, B. Xiao, Z. Wang, W. Tao, S. Shen, L. Huang, J. Zhang, F. Meng, Q. Zhang, L. Gu, W. Zhong, *Adv. Funct. Mater.* **2021**, 31, 2102321.
- [156] W. Li, L. Zhao, X. Jiang, Z. Chen, Y. Zhang, S. Wang, *Adv. Funct. Mater.* **2022**, 2207727.
- [157] K. Mistry, Jalja, R. Lakhani, B. Tripathi, S. Shinde, P. Chandra, *Int. J. Hydrogen Energy* **2022**.
- [158] J. Bonde, P. G. Moses, T. F. Jaramillo, J. K. Nørskov, I. Chorkendorff, *Faraday Discuss.* **2009**, 140, 219.
- [159] C. Tsai, K. Chan, F. Abild-Pedersen, J. K. Nørskov, *Phys. Chem. Chem. Phys.* **2014**, 16, 13156.
- [160] J. Xu, G. Shao, X. Tang, F. Lv, H. Xiang, C. Jing, S. Liu, S. Dai, Y. Li, J. Luo, Z. Zhou, *Nat. Commun.* **2022**, 13, 2193.
- [161] B. Radisavljevic, A. Radenovic, J. Brivio, V. Giacometti, A. Kis, *Nat. Nanotechnol.* **2011**, 6, 147.
- [162] R. Podila, A. Rao, P. Puneet, S. Bhattacharya, S. S. K. Mallineni, A. Srivastava, F. Liu, J. Taha-Tijerina, L. Peña-Parás, D. Maldonado-Cortes, G. Qin, M. Hu, Y. Alaskar, S. Arafin, K. L. Wang, Q. Chi, M. Xue, F. Li, R. Cheung, R. Zhang, G. Sobon, R. Vargas-Bernal, M. Velázquez, T. Alejo, D. López Díaz, B. Martín-García, M. D. M. Moreno, Li, W. Jianghao, L. Guangshe, in *Two-Dimensional Materials-Synthesis, Characterization and Potential Applications*, 1st ed. (Ed: P. K. Nayak), InTech, London **2016**.
- [163] E. Tatarova, N. Bundaleska, J. P. Sarrette, C. M. Ferreira, *Plasma Sources Sci. Technol.* **2014**, 23, 063002.
- [164] S. Li, J. Sun, J. Guan, *Chin. J. Catal.* **2021**, 42, 511.
- [165] X. Zhang, A. Chen, L. Chen, Z. Zhou, *Adv. Energy Mater.* **2021**, 12, 2003841.
- [166] H. Zhang, L. V. Besteiro, J. Liu, C. Wang, G. S. Selopal, Z. Chen, D. Barba, Z. M. Wang, H. Zhao, G. P. Lopinski, S. Sun, F. Rosei, *Nano Energy* **2021**, 79, 105416.
- [167] R. Wang, J. Han, B. Yang, X. Wang, X. Zhang, B. Song, *Chem. Asian J.* **2020**, 15, 3961.
- [168] Q. Liang, Q. Zhang, X. Zhao, M. Liu, A. T. S. Wee, *ACS Nano* **2021**, 15, 2165.
- [169] Z. Lin, B. R. Carvalho, E. Kahn, R. Lv, R. Rao, H. Terrones, M. A. Pimenta, M. Terrones, *2D Mater.* **2016**, 3, 022002.
- [170] M. G. Stanford, P. D. Rack, D. Jariwala, *npj 2D Mater. Appl.* **2018**, 2, 20.
- [171] Y. J. Muhammad, M. A. Alhaji, M. A. Gele, B. Haruna, S. Alhassan, D. Garba, A. Misbahu, *Am. J. Mater. Synth. Process.* **2019**, 4, 9.
- [172] K. S. Novoselov, D. Jiang, F. Schedin, T. J. Booth, V. V. Khotkevich, S. V. Morozov, A. K. Geim, *Proc. Natl. Acad. Sci. U. S. A.* **2005**, 102, 10451.
- [173] K. S. Novoselov, A. K. Geim, S. V. Morozov, D. Jiang, Y. Zhang, S. V. Dubonos, I. V. Grigorieva, A. A. Firsov, *Science* **2004**, 306, 666.
- [174] H. Zhu, X. Gan, A. McCreary, R. Lv, Z. Lin, M. Terrones, *Nano Today* **2020**, 30, 100829.
- [175] S. Rani, M. Sharma, D. Verma, A. Ghanghass, R. Bhatia, I. Sameera, *Mater. Sci. Semicond. Process.* **2022**, 139, 106313.
- [176] E. Pollmann, L. Madau, S. Schumacher, U. Kumar, F. Heuvel, C. vom Ende, S. Yilmaz, S. Güngörmüş, M. Schleberger, *Nanotechnology* **2020**, 31, 505604.
- [177] A. Di Bartolomeo, L. Genovese, T. Foller, F. Giubileo, G. Luongo, L. Croin, S.-J. Liang, L. K. Ang, M. Schleberger, *Nanotechnology* **2017**, 28, 214002.
- [178] F. Urban, F. Giubileo, A. Grillo, L. Lemmo, G. Luongo, M. Passacantando, T. Foller, L. Madau, E. Pollmann, M. P. Geller, D. Oing, M. Schleberger, A. Di Bartolomeo, *2D Mater.* **2019**, 6, 045049.
- [179] C. Lee, H. Yan, L. E. Brus, T. F. Heinz, J. Hone, S. Ryu, *ACS Nano* **2010**, 4, 2695.
- [180] M. Chhowalla, H. S. Shin, G. Eda, L.-J. Li, K. P. Loh, H. Zhang, *Nat. Chem.* **2013**, 5, 263.
- [181] A. Ambrosi, Z. Sofer, M. Pumera, *Small* **2015**, 11, 604.
- [182] T. P. Nguyen, S. Choi, J.-M. Jeon, K. C. Kwon, H. W. Jang, S. Y. Kim, *J. Phys. Chem. C* **2016**, 120, 3929.
- [183] C. Meerbach, B. Klemmed, D. Spittel, C. Bauer, Y. J. Park, R. Hübner, H. Y. Jeong, D. Erb, H. S. Shin, V. Lesnyak, A. Eychmüller, *ACS Appl. Mater. Interfaces* **2020**, 12, 13148.
- [184] L. Tian, H. Qiao, Z. Huang, X. Qi, *Cryst. Res. Technol.* **2021**, 56, 2000165.
- [185] M. Su, W. Zhou, Z. Jiang, M. Chen, X. Luo, J. He, C. Yuan, *ACS Appl. Mater. Interfaces* **2021**, 13, 13055.
- [186] X. Chia, M. Pumera, *ACS Appl. Mater. Interfaces* **2018**, 10, 4937.
- [187] Z. Tian, C. Wei, J. Sun, *Nanoscale Adv.* **2020**, 2, 2220.
- [188] T. A. Shifa, A. Vomiero, *Adv. Energy Mater.* **2019**, 9, 1902307.
- [189] T. P. Nguyen, D. L. T. Nguyen, V.-H. Nguyen, T.-H. Le, Q. V. Ly, D.-V. N. Vo, Q. V. Nguyen, H. S. Le, H. W. Jang, S. Y. Kim, Q. Van Le, *Appl. Surf. Sci.* **2020**, 505, 144574.

- [190] T. Liu, N. Peng, X. Zhang, R. Zheng, M. Xia, H. Yu, M. Shui, Y. Xie, J. Shu, *Nano Energy* **2021**, 79, 105460.
- [191] J. Kibsgaard, Z. Chen, B. N. Reinecke, T. F. Jaramillo, *Nat. Mater.* **2012**, 11, 963.
- [192] H. Li, X. Han, S. Jiang, L. Zhang, W. Ma, R. Ma, Z. Zhou, *Green Energy Environ.* **2022**, 7, 314.
- [193] G. Shao, H. Xiang, M. Huang, Y. Zong, J. Luo, Y. Feng, X.-X. Xue, J. Xu, S. Liu, Z. Zhou, *Sci. China Mater.* **2022**, 65, 1833.
- [194] B. Gao, Y. Zhao, X. Du, Y. Chen, B. Guan, Y. Li, Y. Li, S. Ding, H. Zhao, C. Xiao, Z. Song, *J. Mater. Chem. A* **2021**, 9, 8394.
- [195] P. K. Sahoo, S. R. Bisoi, Y.-J. Huang, D.-S. Tsai, C.-P. Lee, *Catalysts* **2021**, 11, 689.
- [196] P. Zhuang, Y. Sun, P. Dong, W. Smith, Z. Sun, Y. Ge, Y. Pei, Z. Cao, P. M. Ajayan, J. Shen, M. Ye, *Adv. Funct. Mater.* **2019**, 29, 1901290.
- [197] A. D. Nguyen, T. K. Nguyen, C. T. Le, S. Kim, F. Ullah, Y. Lee, S. Lee, K. Kim, D. Lee, S. Park, J.-S. Bae, J. I. Jang, Y. S. Kim, *ACS Omega* **2019**, 4, 21509.
- [198] P. M. Campbell, C. J. Perini, J. Chiu, A. Gupta, H. S. Ray, H. Chen, K. Wenzel, E. Snyder, B. K. Wagner, J. Ready, E. M. Vogel, *2D Mater.* **2017**, 5, 015005.
- [199] B. Huang, F. Tian, Y. Shen, M. Zheng, Y. Zhao, J. Wu, Y. Liu, S. J. Pennycook, J. T. L. Thong, *ACS Appl. Mater. Interfaces* **2019**, 11, 24404.
- [200] C.-C. Cheng, A.-Y. Lu, C.-C. Tseng, X. Yang, M. N. Hedhili, M.-C. Chen, K.-H. Wei, L.-J. Li, *Nano Energy* **2016**, 30, 846.
- [201] J. Xie, H. Zhang, S. Li, R. Wang, X. Sun, M. Zhou, J. Zhou, X. W. D. Lou, Y. Xie, *Adv. Mater.* **2013**, 25, 5807.
- [202] L. Yang, W. Zhou, J. Lu, D. Hou, Y. Ke, G. Li, Z. Tang, X. Kang, S. Chen, *Nano Energy* **2016**, 22, 490.
- [203] J. Zhang, Y. Wang, J. Cui, J. Wu, Y. Li, T. Zhu, H. Kang, J. Yang, J. Sun, Y. Qin, Y. Zhang, P. M. Ajayan, Y. Wu, *J. Phys. Chem. Lett.* **2019**, 10, 3282.
- [204] C. Jian, W. Hong, Q. Cai, J. Li, W. Liu, *Appl. Catal. B* **2020**, 266, 118649.
- [205] S. Mao, Z. Wen, S. Ci, X. Guo, K. K. Ostrikov, J. Chen, *Small* **2015**, 11, 414.
- [206] K. A. Novčić, C. Ifelsberger, S. Ng, M. Pumera, *Nanoscale* **2021**, 13, 5324.
- [207] J. Jang, D. K. Hwang, *J. Korean Phys. Soc.* **2020**, 77, 1008.
- [208] Y. S. Chang, C. Y. Chen, C. J. Ho, C. M. Cheng, H. R. Chen, T. Y. Fu, Y. T. Huang, S. W. Ke, H. Y. Du, K. Y. Lee, L. C. Chao, L. C. Chen, K. H. Chen, Y. W. Chu, R. S. Chen, *Nano Energy* **2021**, 84, 105922.
- [209] W. Wei, Y. Dai, B. Huang, *Phys. Chem. Chem. Phys.* **2017**, 19, 663.
- [210] Z. Peng, X. Chen, Y. Fan, D. J. Srolovitz, D. Lei, *Light Sci. Appl.* **2020**, 9, 190.
- [211] Z. Dai, L. Liu, Z. Zhang, *Adv. Mater.* **2019**, 31, 1805417.
- [212] B. You, M. T. Tang, C. Tsai, F. Abild-Pedersen, X. Zheng, H. Li, *Adv. Mater.* **2019**, 31, 1807001.
- [213] C.-Y. Tu, J. M. Wu, *Nano Energy* **2021**, 87, 106131.
- [214] D. B. Putungan, S.-H. Lin, J.-L. Kuo, *Phys. Chem. Chem. Phys.* **2015**, 17, 21702.
- [215] S. Bolar, S. Shit, N. C. Murmu, P. Samanta, T. Kuila, *ACS Appl. Mater. Interfaces* **2021**, 13, 765.
- [216] T. Rao, H. Wang, Y. Zeng, Z. Guo, H. Zhang, W. Liao, *Adv. Sci.* **2021**, 8, 2002284.
- [217] Y. Jiao, Y. Zheng, K. Davey, S.-Z. Qiao, *Nat. Energy* **2016**, 1, 16130.
- [218] L. Tang, R. Xu, J. Tan, Y. Luo, J. Zou, Z. Zhang, R. Zhang, Y. Zhao, J. Lin, X. Zou, B. Liu, H. Cheng, *Adv. Funct. Mater.* **2021**, 31, 2006941.
- [219] Q. Fu, J. Han, X. Wang, P. Xu, T. Yao, J. Zhong, W. Zhong, S. Liu, T. Gao, Z. Zhang, L. Xu, B. Song, *Adv. Mater.* **2021**, 33, 1907818.
- [220] W. Zhang, X. Liu, T. Liu, T. Chen, X. Shen, T. Ding, L. Cao, L. Wang, Q. Luo, T. Yao, *J. Phys. Chem. C* **2021**, 125, 6229.
- [221] J. Wang, J. He, G. Omololu Odunmbaku, S. Zhao, Q. Gou, G. Han, C. Xu, T. Frauenheim, M. Li, *Chem. Eng. J.* **2021**, 414, 128811.
- [222] L. Yang, Q. Fu, W. Wang, J. Huang, J. Huang, J. Zhang, B. Xiang, *Nanoscale* **2015**, 7, 10490.
- [223] Q. Fu, L. Yang, W. Wang, A. Han, J. Huang, P. Du, Z. Fan, J. Zhang, B. Xiang, *Adv. Mater.* **2015**, 27, 4732.
- [224] C. Ouyang, X. Wang, S. Wang, *Chem. Commun.* **2015**, 51, 14160.
- [225] Y. Zhan, X. Zhou, H. Nie, X. Xu, X. Zheng, J. Hou, H. Duan, S. Huang, Z. Yang, *J. Mater. Chem. A* **2019**, 7, 15599.
- [226] Y.-N. Zhou, Y.-R. Zhu, X.-T. Yan, Y.-N. Cao, J. Li, B. Dong, M. Yang, Q.-Z. Li, C.-G. Liu, Y.-M. Chai, *Chin. J. Catal.* **2021**, 42, 431.
- [227] Y. Li, H. Wang, L. Xie, Y. Liang, G. Hong, H. Dai, *J. Am. Chem. Soc.* **2011**, 133, 7296.
- [228] J. Ye, Z. Yu, W. Chen, Q. Chen, S. Xu, R. Liu, *Carbon* **2016**, 107, 711.
- [229] Y.-R. Zheng, M.-R. Gao, Z.-Y. Yu, Q. Gao, H.-L. Gao, S.-H. Yu, *Chem. Sci.* **2015**, 6, 4594.
- [230] S. Peng, L. Li, X. Han, W. Sun, M. Srinivasan, S. G. Mhaisalkar, F. Cheng, Q. Yan, J. Chen, S. Ramakrishna, *Angew. Chem. Int. Ed.* **2014**, 53, 12594.
- [231] M. Bouroushian, *Electrochemistry of Metal Chalcogenides*, Springer Berlin Heidelberg, Berlin, Heidelberg, **2010**.
- [232] L. A. Burton, A. Walsh, *J. Phys. Chem. C* **2012**, 116, 24262.
- [233] J. M. Skelton, L. A. Burton, A. J. Jackson, F. Oba, S. C. Parker, A. Walsh, *Phys. Chem. Chem. Phys.* **2017**, 19, 12452.
- [234] S. S. Shinde, A. Sami, D.-H. Kim, J.-H. Lee, *Chem. Commun.* **2015**, 51, 15716.
- [235] W. Dong, H. Liu, X. Liu, H. Wang, X. Li, L. Tian, *Int. J. Hydrogen Energy* **2021**, 46, 9360.
- [236] H. Yu, X. Yu, Y. Chen, S. Zhang, P. Gao, C. Li, *Nanoscale* **2015**, 7, 8731.
- [237] M. Kang, C. Lin, H. Yang, Y. Guo, L. Liu, T. Xue, Y. Liu, Y. Gong, Z. Zhao, T. Zhai, K. Zhai, A. Nie, Y. Cheng, Z. Liu, *ACS Appl. Mater. Interfaces* **2021**, 13, 19406.
- [238] J. Zhou, Z. Lin, H. Ren, X. Duan, I. Shakir, Y. Huang, X. Duan, *Adv. Mater.* **2021**, 2004557.
- [239] H. J. Lee, S. W. Lee, H. Hwang, S. I. Yoon, Z. Lee, H. S. Shin, *Mater. Chem. Front.* **2021**, 5, 3396.
- [240] M. Mohl, A. Rautio, G. A. Asres, M. Wasala, P. D. Patil, S. Talapatra, K. Kordas, *Adv. Mater. Interfaces* **2020**, 7, 2000002.
- [241] X. Chia, P. Lazar, Z. Sofer, J. Luxa, M. Pumera, *J. Phys. Chem. C* **2016**, 120, 24098.
- [242] J. Wu, R. Zhao, H. Xiang, C. Yang, W. Zhong, C. Zhang, Q. Zhang, X. Li, N. Yang, *Appl. Catal. B* **2021**, 292, 120200.
- [243] S. A. Patil, N. K. Shrestha, S. Hussain, J. Jung, S.-W. Lee, C. Bathula, A. N. Kadam, H. Im, H. Kim, *J. Hazard. Mater.* **2021**, 417, 126105.
- [244] W. Han, Z. Liu, Y. Pan, G. Guo, J. Zou, Y. Xia, Z. Peng, W. Li, A. Dong, *Adv. Mater.* **2020**, 32, 2002584.
- [245] S. Yu, J. Kim, K. R. Yoon, J.-W. Jung, J. Oh, I.-D. Kim, *ACS Appl. Mater. Interfaces* **2015**, 7, 28116.
- [246] L. Yang, W. Zhou, D. Hou, K. Zhou, G. Li, Z. Tang, L. Li, S. Chen, *Nanoscale* **2015**, 7, 5203.
- [247] X. Chen, G. Liu, W. Zheng, W. Feng, W. Cao, W. Hu, P. Hu, *Adv. Funct. Mater.* **2016**, 26, 8537.
- [248] J. Xu, J. Rong, Y. Zheng, Y. Zhu, K. Mao, Z. Jing, T. Zhang, D. Yang, F. Qiu, *Electrochim. Acta* **2021**, 385, 138438.
- [249] J. Li, A. Listwan, J. Liang, F. Shi, K. Li, J. Jia, *Chem. Eng. J.* **2021**, 422, 130100.
- [250] D. Ö. Özgür, G. Özkan, O. Atakol, H. Çelikkan, *ACS Appl. Energy Mater.* **2021**, 4, 2398.
- [251] L. Najafi, S. Bellani, R. Oropesa-Nuñez, A. Ansaldi, M. Prato, A. E. Del Rio Castillo, F. Bonaccorso, *Adv. Energy Mater.* **2018**, 8, 1703212.
- [252] D. Vikraman, S. Hussain, M. Ali, K. Karuppasamy, P. Santhoshkumar, J.-H. Hwang, J. Jung, H.-S. Kim, *J. Alloys Compd.* **2021**, 868, 159272.

- [253] W. Liao, S. Zhao, F. Li, C. Wang, Y. Ge, H. Wang, S. Wang, H. Zhang, *Nanoscale Horiz.* **2020**, *5*, 787.
- [254] K. Cho, J. Pak, S. Chung, T. Lee, *ACS Nano* **2019**, *13*, 9713.
- [255] R. Luo, W. W. Xu, Y. Zhang, Z. Wang, X. Wang, Y. Gao, P. Liu, M. Chen, *Nat. Commun.* **2020**, *11*, 1011.
- [256] Y. Zhao, K. Xu, F. Pan, C. Zhou, F. Zhou, Y. Chai, *Adv. Funct. Mater.* **2017**, *27*, 1603484.
- [257] J. Peng, X. Chen, W.-J. Ong, X. Zhao, N. Li, *Chem* **2019**, *5*, 18.
- [258] C.-A. Chen, C.-L. Lee, P.-K. Yang, D.-S. Tsai, C.-P. Lee, *Catalysts* **2021**, *11*, 151.
- [259] Q. Xu, H. Jiang, H. Zhang, Y. Hu, C. Li, *Appl. Catal. B.* **2019**, *242*, 60.
- [260] L. Jia, C. Li, Y. Zhao, B. Liu, S. Cao, D. Mou, T. Han, G. Chen, Y. Lin, *Nanoscale* **2019**, *11*, 23318.
- [261] X. Gan, L. Y. S. Lee, K. Wong, T. W. Lo, K. H. Ho, D. Y. Lei, H. Zhao, *ACS Appl. Energy Mater.* **2018**, *1*, 4754.
- [262] S. Geng, Y. Ji, B. Jiang, W. Zhu, K. Yin, M. Shao, F. Liao, H. Shi, Y. Cheng, Y. Li, Q. Shao, *ACS Appl. Nano Mater.* **2022**, *5*, 1377.
- [263] G. Gao, Y. Jiao, F. Ma, Y. Jiao, E. Wacławik, A. Du, *J. Phys. Chem. C* **2015**, *119*, 13124.
- [264] S. Wang, Y. Li, Y. Hu, X. Zhou, M. Zhang, X. Jia, Y. Yang, B.-L. Lin, G. Chen, *ACS Appl. Energy Mater.* **2022**, *5*, 11705.
- [265] M. A. Lukowski, A. S. Daniel, F. Meng, A. Forticaux, L. Li, S. Jin, *J. Am. Chem. Soc.* **2013**, *135*, 10274.
- [266] W. He, X. Zheng, J. Peng, H. Dong, J. Wang, W. Zhao, *Chem. Eng. J.* **2020**, *396*, 125227.
- [267] J. Yuan, J. Wu, W. J. Hardy, P. Loya, M. Lou, Y. Yang, S. Najmaei, M. Jiang, F. Qin, K. Keyshar, H. Ji, W. Gao, J. Bao, J. Kono, D. Natelson, P. M. Ajayan, J. Lou, *Adv. Mater.* **2015**, *27*, 5605.
- [268] J. Wang, M. Yan, K. Zhao, X. Liao, P. Wang, X. Pan, W. Yang, L. Mai, *Adv. Mater.* **2017**, *29*, 1604464.
- [269] Y. Shi, J. Wang, C. Wang, T.-T. Zhai, W.-J. Bao, J.-J. Xu, X.-H. Xia, H.-Y. Chen, *J. Am. Chem. Soc.* **2015**, *137*, 7365.
- [270] J. Yin, J. Jin, H. Lin, Z. Yin, J. Li, M. Lu, L. Guo, P. Xi, Y. Tang, C. Yan, *Adv. Sci.* **2020**, *7*, 1903070.



Aniruddha Mondal received his B.Sc. (H) degree in Chemistry Honors from Burdwan University, M.Sc. in Organic Chemistry from Nagpur University, respectively. He joined as Junior Research Fellow (JRF) in Council of Scientific and Industrial Research-Central Salt and Marine Chemicals Research Institute (CSIR-CSMCRI), where he was awarded Ph.D. degree in 2018 in Chemical Science. He joined as Post-Doctoral Fellow in Tatung University, Taipei, Taiwan in MOST Post-Doctoral Fellowship for 1.6 years. Currently, He is working with Prof. Alberto Vomiero in Luleå University of Technology, Luleå, Sweden. His research motivation on the development of nano-structured materials and their application in energy conversion and storage, electrocatalysis, and photocatalysis.



Alberto Vomiero is a chair professor of Experimental Physics at the Department of Engineering Sciences and Mathematics, Luleå University of Technology, Sweden and a professor of Industrial Engineering at the Department of Molecular Sciences and Nanosystems, Ca' Foscari University of Venice, Italy. He is leading a multidisciplinary group focusing on the development of advanced nanomaterials for energy and environmental applications, including solar cells, water splitting, and photocatalysis. He is a former Marie Curie International Outgoing Fellow of the European Commission, Fellow of the Swedish Foundations, of the Royal Society of Chemistry, and several other Societies.